



HAL
open science

Stomatal regulators are co-opted for seta development in the astomatous liverwort *Marchantia polymorpha*

Kenta Moriya, Makoto Shirakawa, Jeanne Loue-Manifel, Yoriko Matsuda, Yen-Ting Lu, Kentaro Tamura, Yoshito Oka, Tomonao Matsushita, Ikuko Hara-Nishimura, Gwyneth Ingram, et al.

► To cite this version:

Kenta Moriya, Makoto Shirakawa, Jeanne Loue-Manifel, Yoriko Matsuda, Yen-Ting Lu, et al.. Stomatal regulators are co-opted for seta development in the astomatous liverwort *Marchantia polymorpha*. 2023. hal-03812124

HAL Id: hal-03812124

<https://cnrs.hal.science/hal-03812124>

Preprint submitted on 27 Oct 2023

HAL is a multi-disciplinary open access archive for the deposit and dissemination of scientific research documents, whether they are published or not. The documents may come from teaching and research institutions in France or abroad, or from public or private research centers.

L'archive ouverte pluridisciplinaire **HAL**, est destinée au dépôt et à la diffusion de documents scientifiques de niveau recherche, publiés ou non, émanant des établissements d'enseignement et de recherche français ou étrangers, des laboratoires publics ou privés.

1 **Stomatal regulators are co-opted for the development of setae in the**
2 **astomatous liverwort *Marchantia polymorpha***

3
4 **Authors**

5 Kenta C. Moriya¹, Makoto Shirakawa², Jeanne Loue-Manifel^{3,4}, Yoriko Matsuda⁵, Yen-
6 Ting Lu^{2,4}, Kentaro Tamura⁶, Yoshito Oka¹, Tomonao Matsushita¹, Ikuko Hara-
7 Nishimura⁷, Gwyneth Ingram³, Ryuichi Nishihama^{5,8}, Justin Goodrich⁴, Takayuki
8 Kohchi⁵, Tomoo Shimada^{1,*}

9
10 **Affiliations**

11 ¹Graduate School of Science, Kyoto University, Kyoto 606-8502, Japan

12 ²Graduate School of Biological Sciences, Nara Institute of Science and Technology
13 (NAIST), Ikoma 630-0192, Japan

14 ³Laboratoire Reproduction et Développement des Plantes, ENS de Lyon, CNRS,
15 INRAE, UCB Lyon 1, Lyon 69342, France

16
17 ⁴Institute of Molecular Plant Sciences, University of Edinburgh, Daniel Rutherford
18 Building, Max Born Crescent, Edinburgh EH9 3BF, UK

19 ⁵Graduate School of Biostudies, Kyoto University, Kyoto 606-8502, Japan

20 ⁶School of Food and Nutritional Sciences, University of Shizuoka, Shizuoka 422-8526,
21 Japan

22 ⁷Faculty of Science and Engineering, Konan University, Kobe 658-8501, Japan

23 ⁸Department of Applied Biological Science, Faculty of Science and Technology, Tokyo
24 University of Science, Noda 278-8510, Japan

25
26 *Correspondence: tshimada@gr.bot.kyoto-u.ac.jp

27
28 **Abstract**

29 The evolution of special types of cells requires the acquisition of new gene regulatory
30 networks controlled by transcription factors (TFs). In stomatous plants, stomatal
31 formation is regulated by a TF module formed by subfamilies Ia and IIIb basic helix-
32 loop-helix TFs (Ia-IIIb bHLH); however, how this module evolved during land plant
33 diversification remains obscure. Here, we show that, in the astomatous liverwort
34 *Marchantia polymorpha*, a Ia-IIIb bHLH module regulates the development of a unique
35 sporophyte tissue, the seta, which is found in mosses and liverworts. The sole Ia bHLH
36 gene, MpSETA, and a IIIb bHLH gene, MpICE2, regulate cell division and/or
37 differentiation of seta lineage cells. MpSETA can partially replace the stomatal function
38 of Ia bHLH TFs in *Arabidopsis thaliana*, suggesting that a common regulatory
39 mechanism underlies setal and stomatal formation. Our findings reveal the co-option of
40 a Ia-IIIb bHLH TF module for regulating cell fate determination and/or cell division of
41 distinct types of cells during the evolution of land plant.

43 Land plants developed unique types of cells and tissues to adapt to the terrestrial
44 environment during evolution^{1,2}. The acquisition of novel cells or tissues leading to
45 complex body plans is related to the diversification of transcription factors (TFs)^{3,4}. Basic
46 helix-loop-helix (bHLH) TFs represent a TF superfamily that plays key roles in cell fate
47 determination and cell division during the development of eukaryotes. In land plants, the
48 number of genes encoding bHLH TFs has increased compared with those of chlorophyte
49 and charophyte algae, suggesting that bHLH TFs are involved in terrestrial adaptation⁵.
50 For example, the acquisition of stomata, a special tissue for gas exchange on the epidermis,
51 is an important adaptation of plants to terrestrial environments; previous studies have
52 revealed that stomatal formation is regulated by bHLH TFs as master TFs⁶⁻⁹. In
53 *Arabidopsis thaliana*, three TFs belonging to subfamily Ia (SPEECHLESS [SPCH],
54 MUTE, and FAMA)⁶⁻⁸ form heterodimers with subfamily IIIb TFs (ICE1, also known as
55 SCREAM [SCRM], and ICE2, also known as SCRM2) to promote stomatal formation by
56 regulating downstream gene expression⁹. The molecular mechanism of stomatal
57 formation by Ia and IIIb bHLH TFs is conserved in the moss *Physcomitrium patens*, in
58 which stomata play an important role in spore dispersal by promoting dehydration and
59 dehiscence of the sporangium^{10,11}.

60 Recent studies revealed that a gene encoding a Ia bHLH is present in the genome
61 of the astomatous liverwort *Marchantia polymorpha*^{4,12-14}. Despite the importance of Ia
62 bHLH in stomatal development, its function in plants lacking stomata has not yet been
63 explored. Here, we report that the Ia bHLH protein, designated as MpSETA, is a master
64 regulator of the formation of the seta, which is a diploid tissue involved in long-distance
65 spore dispersal in *M. polymorpha*. Furthermore, we show that Ia and IIIb bHLH positively
66 regulate setal formation by heterodimerization, similar to their role in stomatal formation
67 in other land plants. This outcome not only advances our understanding of the
68 mechanisms of the evolution of plant tissue formation but also provides new insights into
69 the co-option of gene expression regulatory networks (GRNs).

71 Results

72 MpSETA is the sole Ia bHLH protein in *M. polymorpha*.

73 To identify Ia bHLH coding genes in *M. polymorpha*, we constructed a phylogenetic tree
74 of Ia bHLH proteins from various plant species using the bHLH domain and a C-terminal
75 conserved domain called SMF (also known as the ACT-like domain)^{15,16} (Fig. 1a and
76 Extended Data Fig. 1). Our phylogenetic analysis suggested that MpBHLH35
77 (Mp2g04160) is the sole Ia bHLH in *M. polymorpha* (Fig. 1a). We named this gene
78 MpSETA based on its specific expression in the seta tissue of the sporophyte (see below).
79 Multiple alignments of bHLH proteins revealed that the amino acid residues predicted to
80 be important for E-box (CANNTG) binding and bHLH dimerization are highly conserved
81 in MpSETA, although the amino acid sequence of the bHLH domain of MpSETA is
82 relatively divergent compared to other Ia bHLH (Extended Data Fig. 1b). Additionally,
83 we found partial sequences of two MpSETA related genes (LcSETA1 and LcSETA2) in the
84 genome of the Marchantiopsida liverwort *Lunularia cruciata*¹⁷, although there is no
85 evidence that these putative MpSETA-like genes are expressed and are functional in this
86 species (Fig. 1a and Extended Data Fig. 1b-c). The amino acid sequences of the bHLH
87 and SMF domains are well conserved between MpSETA and LcSETA1. Thus, we can
88 conclude that Ia bHLH genes are conserved in the genome of Marchantiales liverworts.

89 Since the amino acid sequence of MpSETA is divergent, it is unclear if MpSETA

90 has similar properties as the other Ia bHLH proteins. Therefore, we investigated whether
91 MpSETA can act as a stomatal regulator replacing AtSPCH, AtMUTE, or AtFAMA. In
92 this context, MpSETA was expressed under the native promoters of AtSPCH, AtMUTE,
93 and AtFAMA in *spch-3*, *mute-2*, and *fama-1* backgrounds, respectively (Fig. 1b and
94 Extended Data Fig. 2a,b). Even though *mute-2* results in arrested meristemoids (self-
95 renewing stomatal precursors), a few stomata were formed in *mute-2* expressing MpSETA
96 (Fig. 1b) (2.67 ± 1.56 and 2.33 ± 1.72 per abaxial side of the cotyledon in the lines #8-4
97 and #10-11, respectively [mean \pm s.d.; $n = 12$]). Notably, hydathode pores (a modified
98 form of stomatal pores) were often found in these lines. This might be due to the high
99 expression activity of the AtMUTE promoter in the hydathode of the cotyledons¹⁸.
100 MpSETA also exhibited the potential to rescue *fama-1*. *A. thaliana fama* mutant displays
101 caterpillar-like stomatal-lineage cells called “*fama* tumors,” where the terminal
102 symmetric division occurs more than once⁸. In *fama-1* expressing MpSETA, excess cell
103 divisions in stomatal lineage were suppressed, although no mature stomata were formed
104 (Extended Data Fig. 2b,c). Neither stomata nor stomatal-lineage cells were found in *spch-3*
105 expressing MpSETA (Extended Data Fig. 2a). These results showing that MpSETA is
106 partially functional in stomatal-cell division and differentiation in *A. thaliana* suggest that
107 it can interact with AtICE1 and AtSCRM2. Therefore, we tested this ability in yeast two-
108 hybrid assays and bimolecular fluorescent complementation (BiFC) assays. We found that
109 MpSETA physically interacted with AtICE1 and AtSCRM2 (Extended Data Fig. 2d,e).
110 Thus, our findings indicate that MpSETA from the astomatous liverwort is a bona fide Ia
111 bHLH TF, albeit its amino acid sequence is divergent.

112

113 **MpSETA is preferentially expressed in developing sporophyte.**

114 To investigate the expression pattern of MpSETA in *M. polymorpha*, we reanalyzed the
115 public RNA-seq dataset from several organs^{4,19-22} and found that MpSETA was
116 preferentially expressed in the diploid sporophyte, whereas its expression level was low
117 in the haploid gametophyte (Fig. 2a).

118 We examined in detail the expression pattern of MpSETA by characterizing the
119 different stages of development in the *M. polymorpha* sporophyte (Fig. 2b-c); in wild type,
120 sporophytes are divided into three tissues: foot, seta, and sporangium (Fig. 2b). The foot
121 plays a key role in nutrient transport between the gametophyte and the sporophyte, while
122 the seta, which consists of files of elongated cells that form a stalk suspending the
123 sporangium, plays a pivotal role in spore dispersal²³⁻²⁵. After late spore maturation in
124 sporophyte development, the seta extends through elongation of its cells and thrusts the
125 sporangium outwards, causing it to break through the surrounding calyptra and
126 pseudoperianth, which are tissues derived from the archegonium and the archegoniophore,
127 respectively, to protect the sporophyte during development²³⁻²⁵. As a result, spores are
128 dispersed after sporangium dehiscence by desiccation. Based on the unique
129 developmental events as shown in previous studies^{22,23,26}, we divided the development of
130 the sporophyte into 10 stages, as follows (Fig. 2c,d): (I) 2-cell stage with the epibasal cell
131 (the upper cell that forms the foot and the seta) and the hypobasal cell (the lower cell that
132 forms the sporangium), (II) 4 or 8-cell stage, (III) early-globular stage with a distinct
133 amphithecium (the outermost tissue that forms the capsule wall) and the endothecium (the
134 inner archesporial tissue); (IV) late-globular stage; (V) archesporial-tissue stage with the
135 visible differentiated foot, seta, and archesporial tissues; (VI) sporogenous-cell stage with
136 elaterocytes and sporogenous cells, which are the precursors of elaters and sporocytes

137 (spore mother cells); (VII) sporocyte stage; (VIII) spore-tetrad stage (after meiosis); (IX)
138 matured stage; (X) seta-elongated stage. Note that seta and foot are established between
139 stages V and IX. In stage VIII, we anatomically observed proliferative (symmetric) cell
140 divisions in the seta region (Fig. 2e). Moreover, cell division activity was detected not in
141 the foot but rather in the seta of sporophytes between stages VII and VIII using a G2-M
142 phase reporter line, *proMpCYCB;1:Dbox-GUS*²⁷ (Fig. 2f). Thus, we concluded that the cell
143 files in the seta are established by a few proliferative cell divisions of the putative “seta
144 mother cells” in the later developmental stage.

145 We detected the promoter activity of *MpSETA* in the sporophyte by generating
146 transformants expressing the β -glucuronidase gene (*GUS*) under the control of the
147 *MpSETA* promoter (*proMpSETA:GUS*). *GUS* activity was found in developing
148 sporophytes between stages IV and VII, especially in seta, whereas no *GUS* activity was
149 found in stages VIII and IX (Fig. 2g). In gametophytic tissues, *GUS* signals were detected
150 only in young antheridia (Extended Data Fig. 3). These findings suggest that *MpSETA* is
151 expressed early in seta development and may regulate seta cell division and/or
152 differentiation rather than the elongation of seta cells.

153 ***Mpseta*^{ko} mutants show defects in setal formation in the sporophyte.**

154 We generated loss-of-function mutants of *MpSETA* by homologous recombination-
155 mediated gene targeting to reveal the function of *MpSETA* *in vivo*²⁸. Therefore, we
156 obtained two independent *MpSETA* knock-out lines (*Mpseta-1*^{ko} and *Mpseta-2*^{ko}) in
157 which the genomic regions encoding the bHLH domain were replaced with a
158 hygromycin-resistance gene cassette (Extended Data Fig. 4a-c). We confirmed the loss of
159 the full-length transcripts of the *MpSETA* gene by reverse-transcription polymerase chain
160 reaction (RT-PCR) analysis of homozygous mutant sporophytes produced from crosses
161 between *Mpseta-1*^{ko} or *Mpseta-2*^{ko} males and females (Extended Data Fig. 4d). Although
162 *MpSETA* reporter gene expression was found in the developing antheridia (Extended Data
163 Fig. 3), no obvious phenotype was observed during sperm formation in *Mpseta*^{ko} lines
164 (Extended Data Fig. 4e), and mutant males were fertile.

165 We crossed males and females of *Mpseta*^{ko} and compared the resulting
166 sporophytes with those of the wild type to investigate phenotypes of *Mpseta*^{ko} mutants in
167 the diploid generation. In longitudinal sections of mature sporophytes of *Mpseta*^{ko}, we
168 found anatomical defects in the development of setal cells (Fig. 3a,b). We did not observe
169 any elongated seta cells or cell files of seta cells in *Mpseta*^{ko} mutants. The SF/SP ratio (a
170 ratio of the length from the foot to the proximal side of sporangium to the total sporophyte
171 length) and the number of cells around the seta region were significantly reduced in
172 *Mpseta*^{ko} compared with wild type (Fig. 3c,d). Detailed analysis of earlier stages of
173 sporophyte development revealed that defects in *Mpseta-1*^{ko} setae could be found even at
174 stage VI, the earliest stage at which putative seta mother cells are unequivocally
175 recognized (Fig. 3e). Despite the obvious loss of setae, spores and other sporophytic
176 tissues were normally formed in *Mpseta-1*^{ko} (Fig. 3e,f). We concluded that *Mpseta*^{ko}
177 mutants have defects in the differentiation from putative seta precursor cells to seta
178 mother cells, which prevents the induction of the subsequent proliferative cell divisions.
179 At one-month postfertilization, the wild-type sporangia were pushed out of the calyptras.
180 By contrast, *Mpseta*^{ko} sporangia remained buried inside the calyptras, presumably due to
181 the defects in seta development, and hence were not exposed to the outside (Fig. 3g).
182 Since sporangia are completely wrapped by the calyptras and pseudoperianths, spore
183

184 dispersal does not occur unless the sporangia are pushed out of the calyptras by elongation
185 of seta cells²⁹. In genetic complementation experiments, we generated a transgenic line
186 having the genomic region of MpSETA introduced into Mpseta-1^{ko} (gMpSETA Mpseta-
187 1^{ko}). The sporophytes obtained by crossing these complemented lines had normal setae,
188 and their sporangia were pushed out of the calyptra as in the wild type (Fig. 3).
189 Consequently, these results suggest that MpSETA is essential for setal formation and spore
190 dispersal in *M. polymorpha*.

191 **MpICE2 physically interacts with MpSETA and regulates setal development.**

192 Since the interaction between Ia and IIIb bHLHs is evolutionarily conserved^{9,10,30}, we
193 examined whether Ia bHLH and IIIb bHLH physically interact with each other in *M.*
194 *polymorpha*. We performed phylogenetic analyses to find IIIb bHLH genes in *M.*
195 *polymorpha* and identified two genes encoding IIIb bHLH proteins in the genome of *M.*
196 *polymorpha*, both of which are orthologous to AtICE1 and AtSCRM2 (Extended Data Fig.
197 5). We named these genes MpICE1 (Mp4g04910) and MpICE2 (Mp4g04920). The amino
198 acid sequences of the bHLH and ACT-like domains of IIIb bHLHs were highly conserved
199 among land plants (Extended Data Fig. 6). In addition, two putative IIIb bHLH-encoding
200 genes, LcICE1 and LcICE2, were found in the genome of *L. cruciata* (Extended Data
201 Figs. 5 and 6).
202

203 Reanalyzing public RNA-seq data revealed high expression of MpICE2 at 13
204 days postfertilization in young sporophytes (from stage III to stage IV)¹⁹, in which
205 putative seta mother cells were dividing and differentiating, while the expression level of
206 MpICE1 was almost constant in all tissues (Fig. 4a). Thus, we assumed that MpICE2 may
207 predominantly function in cooperation with MpSETA during seta cell formation rather
208 than MpICE1. We expressed *Citrine* (a yellow fluorescent protein; YFP), *GUS*, and
209 nuclear localization-signal (*NLS*) fusion gene (*Citrine-GUS-NLS*) under the control of the
210 MpICE2 promoter to confirm the tissue/cell-level expression pattern of MpICE2 in the
211 sporophyte. In this line, GUS signals were detected overall in stages IV and V sporophytes,
212 specifically in the seta and foot in stages VI-VIII sporophytes, and only in the foot in
213 mature sporophytes together with Citrine and GUS signals in gametophytic tissues
214 (Extended Data Fig. 7).

215 We performed yeast two-hybrid assays using full-length MpSETA in pairwise
216 combinations with MpICE2 to test the interaction between MpSETA and MpICE2; in this
217 context, a physical interaction was observed (Fig. 4b). Additionally, BiFC assay was used
218 to test the interaction between these bHLH TFs. YFP signals were detected in the nuclei
219 of *Nicotiana benthamiana* leaves coexpressing MpSETA-nYFP and MpICE2-cYFP (Fig.
220 4c). These results suggest that MpSETA has the potential to interact with MpICE2 in *M.*
221 *polymorpha*.

222 We generated two independent genome-edited lines using the CRISPR/Cas9
223 system (Mpice2-2^{ge} and Mpice2-6^{ge}) to assess the function of MpICE2^{31,32}. The first one
224 retained two amino acid substitutions (L503H and M504L) that were predicted to be
225 important for the DNA-binding activity of the bHLH domain³³, while the second had a
226 frame-shift mutation that caused deletion of the C-terminal half of the bHLH domain and
227 the whole ACT-like domain (Extended Data Fig. 8). In these Mpice2 mutants, the setae
228 of sporophytes were not formed (Fig. 4d,e) and the number of cells between foot and
229 sporangium was significantly reduced (Fig. 4f,g). Additionally, we found that the number
230 of cells in the seta region of Mpice2-2^{ge} was higher than that of Mpice2-6^{ge} (Fig. 4g). This

231 is probably because the predicted translational product of *Mpice2-2^{se}* has a two-amino
232 acid substitution in the bHLH domain, and might be partially functional in comparison
233 with the null allele *Mpice2-6^{se}*. In both *Mpice2^{se}* mutants, the sporophytes did not emerge
234 outside of the protective organs derived from the archegonia, similar to the *Mpseta^{ko}*
235 mutants (Fig. 4h). Since the single mutants of *Mpice2^{se}* showed almost the same
236 phenotype as that of the *Mpseta^{ko}* mutants, *MpICE1* may not be functionally redundant
237 with *MpICE2* at least in the setal formation. The *Mpice2^{se}* phenotype in the setal region
238 was completely suppressed by introducing the genomic region of *MpICE2* into *Mpice2-*
239 *6^{se}* (Fig. 4d-h). Therefore, we can conclude that the MpSETA-MpICE2 heterodimer plays
240 an important role in the setal development of *M. polymorpha*.

241 Next, we tested if *MpICE2* can enhance the rescue of the stomatal phenotype of
242 *mute-2* by *proAtMUTE:MpSETA*. Overexpression of *MpICE2* in *proAtMUTE:MpSETA*
243 *mute-2* did not enhance stomatal formation (Extended Data Fig. 9a) (3.63 ± 3.16 and
244 2.64 ± 1.41 per abaxial side of the cotyledon in the lines #8-4 and #10-11, respectively
245 [mean \pm s.d.; $n = 11$]). Therefore, the MpSETA-MpICE2 heterodimer does not appear to
246 regulate the expression of stomatal genes in *A. thaliana*. In addition, the expression of
247 *MpICE1* or *MpICE2* under the control of the *AtICE1* promoter in *ice1-2 scrm2-1* mutants
248 failed to cause stomatal-lineage cell formation (Extended Data Fig. 9b). Therefore,
249 *MpICE1* and *MpICE2* cannot act with *AtSPCH* to regulate stomatal formation in *A.*
250 *thaliana*, despite the similarity of their amino acid sequences with *AtICE1* (Extended
251 Data Fig. 6).

252 Discussion

253 In this article, we showed that two transcription factors, MpSETA (Ia bHLH) and MpICE2
254 (IIIb bHLH), play a pivotal role in controlling the formation of the diploid tissue seta in
255 the sporophyte of *M. polymorpha*, which is an astomatous liverwort (Figs. 3 and 4).
256 Similarly, in other non-liverwort land plants, a module formed by the subfamilies Ia and
257 IIIb bHLH TFs regulates GRNs in stomatal development². *MpSETA* could partially
258 complement the defects of *A. thaliana mute* and *fama*, suggesting similar properties of Ia
259 bHLH TFs from *M. polymorpha* and *A. thaliana*. However, *MpSETA* was unable to
260 complement the *spch* mutant (Fig. 1b and Extended Data Fig. 2). These results are
261 consistent with the previous hypothesis stating that the ancestral Ia bHLH proteins had a
262 MUTE- and FAMA-like function^{34,35}. Although the nature of *MpSETA* expressing cells is
263 still unknown, *MpSETA* may function as a regulator of cell differentiation and asymmetric
264 cell division during setal formation, similar to its role in stomatal formation (Fig. 5a).

265 Although stomata and setae are completely different morphologically, they both
266 play a common role in promoting sporangial dehiscence and spore dispersal. In mosses
267 and hornworts, stomata are present in the epidermis of the sporangia and function in the
268 desiccation of the sporangia by gas exchange to promote its dehiscence and spore
269 dispersal^{25,36}. In *A. thaliana*, *AtICE1* controls stomatal development on anther epidermis
270 and can regulate dehydration and dehiscence of the anther³⁷. However, the seta is the
271 tissue that supports the sporangia and has a role through cell elongation in thrusting the
272 sporangia outside the surrounding maternal tissues to permit long-distance dispersal of
273 spores^{24,25}. In this study, we found that the lack of setae in *Mpseta^{ko}* and *Mpice2^{se}* mutants
274 prevented sporangia dehiscence and spore dispersal due to the inability of the sporangia
275 to break through the protective organs around it (Figs. 3 and 4). Thus, the Ia-IIIb bHLH
276 module has a common role in the development of the tissues involved in spore or pollen
277

278 dispersal.

279 Previous research suggested that land plant evolution occurred through the reuse
280 and/or modification of preexisting GRNs^{20,38-43}. Here, we hypothesize that the Ia-IIIb
281 bHLH module was primarily used in stomatal formation and secondarily co-opted to setal
282 formation in the common ancestor of “Setaphyta” (Fig. 5b). Since only mosses and
283 liverworts have setae, a mosses-liverworts clade is called Setaphyta^{1,44,45}. However, the
284 process of setal development differs between mosses and liverworts; whereas a transient
285 intercalary meristem, called the seta meristem, produces seta in mosses, the body plan,
286 including seta, foot, and sporangium, is established by formative cell division at an early
287 stage in liverworts²⁵. Therefore, whether the Ia-IIIb bHLH module is involved in the
288 formation of seta in mosses, such as *P. patens*^{46,47}, should be tested.

289 In *A. thaliana*, the AtFAMA-AtICE1 heterodimer regulates not only the
290 development of stomata but also of myrosin idioblasts, which are adjacent to vascular
291 tissues and contribute to defense against herbivores^{41,48,49}. Since myrosin cells are present
292 only in the Brassicales, the AtFAMA-AtICE1 module for stomatal formation was co-
293 opted for myrosin cell development during the evolution of Brassicales (Fig. 5b). The
294 AtFAMA-AtICE1 module is thought to regulate the expression of different genes in
295 stomatal and myrosin cell lineages^{41,48,49}; however, the detailed mechanism is not yet
296 known. Liverworts have already lost several stomatal-related genes^{4,50}, such as the
297 leucine-rich-repeat receptor-like gene *TOO MANY MOUTHS (TMM)* and the secreted
298 peptide gene *EPIDERMAL PATTERNING FACTOR 1/2 (EPF1/2)*. The mechanisms
299 underlying the development of setal-cell lineage might be different from the ones related
300 to stomatal-cell lineages. AtMUTE directly regulates cell-cycle related genes (cyclin and
301 cyclin-dependent kinase genes) and several stomatal-related TF genes⁵¹, and AtSPCH
302 directly regulates the stomatal-related genes and brassinosteroid pathway genes⁵². In *M.*
303 *polymorpha*, orthologues of many of the Ia-IIIb bHLH target genes, including *CYCB*,
304 *CYCD*, *CDKB*, *ERECTA*, and BZR/BES family TF genes, are conserved⁴. RNA-seq and
305 ChIP-seq analyses could identify genes that function downstream of the MpSETA-
306 MpICE2 module, and help to clarify whether other stomatal formation-related genes are
307 involved in setal formation.

308 Are *SMF* genes and/or MpSETA orthologs conserved in the Jungermanniopsida
309 or Haplomitriopsida liverworts? A BLAST search of 1,000 plant transcriptomes
310 (OneKP)⁵³, using AtFAMA as query, revealed the absence of Ia bHLH TFs in liverworts
311 except for MpSETA. Since the liverwort transcriptome samples used in OneKP often do
312 not contain sporophytes, it is difficult to detect genes that are specifically or transiently
313 expressed in developing sporophytes, such as Ia bHLH. Since the Ricciaceae species have
314 lost seta, it will be important to investigate whether these species have Ia bHLH and
315 whether the Ia bHLHs are functional to understand the evolution of setae. Genome
316 analyses of various plant species in the future could be useful to understand the
317 relationship between Ia bHLH diversification and stomata/seta formation.

318

319 **Methods**

320 **Phylogenetic analysis**

321 The classifications of bHLH are according to Pires and Dolan⁵. Amino acid sequence
322 information was retrieved from MarpolBase (<https://marchantia.info>), Phytozome v.13
323 (<https://phytozome-next.jgi.doe.gov/>), OneKP (<https://db.engb.org/onekp/>), TAIR
324 (<http://www.arabidopsis.org/>), and NCBI

325 (<https://www.ncbi.nlm.nih.gov/genome/?term=PRJNA701193>). The bHLH domain and
326 C-terminal ACT-like domain were aligned using MAFFT⁵⁴ v.6.864
327 (<https://www.genome.jp/tools-bin/mafft>) with the default parameters, and the alignment
328 gaps were removed manually. Amino acid sequences were visualized with Jalview⁵⁵
329 v.2.11.2.1. BLAST searches of NCBI (<https://blast.ncbi.nlm.nih.gov/Blast.cgi>) were used
330 to predict the amino acids important for nucleotide binding and dimer formation in the
331 bHLH domains. Phylogenetic tree constructions were performed using the maximum-
332 likelihood algorithm on MEGA 7⁵⁶ with the JTT+G+I substitution model for Ia and
333 LG+G+I substitution model for IIIb bHLH. Bootstrap analyses with 1000 replicates were
334 performed in each analysis to assess the statistical support for the topology. Subfamilies
335 III(a+c) and III(d+e) bHLHs were chosen as the outgroup of the phylogeny for Ia and IIIb
336 bHLH, respectively.

337

338 **Plant materials and growth condition**

339 Male and female accessions of *M. polymorpha* L., Takaragaike-1 (Tak-1), and Tak-2,
340 respectively, were maintained asexually. A female progeny backcrossed to Tak-1 for three
341 backcross generations (BC3-38) and male Tak-1 were used as wild type. Gemmae and
342 thalli were cultured on half-strength Gamborg's B5 media containing 1% (w/v) agar and
343 1% (w/v) sucrose under 50-60 $\mu\text{mol photons m}^{-2} \text{s}^{-1}$ continuous white light at 22°C. To
344 induce gametangiophore development, 10 to 12-day-old thalli were transferred to 16-h-
345 light/8-h-dark conditions with 50-60 $\mu\text{mol photons m}^{-2} \text{s}^{-1}$ white light and 50-60 μmol
346 $\text{photons m}^{-2} \text{s}^{-1}$ far-red light emitted from diodes (IR LED STICK 18W, Namoto) at 18°C
347 and incubated for 1 month.

348 The *Arabidopsis thaliana* Columbia-0 (Col-0) accession was used as wild type
349 except for *mute-2* where Wassilewskija-4 (Ws-4) was used. Seeds were surface sterilized
350 with 70% ethanol and then sown onto half-strength MS media containing 0.5% (w/v)
351 gellan gum and 1% (w/v) sucrose. The seeds were incubated at 22°C under 50-60 μmol
352 $\text{photons m}^{-2} \text{s}^{-1}$ continuous white light.

353

354 **Complementation tests of *A. thaliana* stomatal defective mutants**

355 T-DNA insertion mutants *spch-3* (SAIL_36_B06) and *fama-1* (SALK_100073) were
356 obtained from the Arabidopsis Biological Resource Center (ABRC); *mute-2*
357 (FLAG_225D03) from the French National Institute for Agricultural Research (INRA).
358 *ice1-2 scrm2-1*⁹ was provided by K.U. Torii. To construct *proAtSPCH:MpSETA*, firstly the
359 *AtSPCH* promoter (2,572 bp upstream of the translational initiation site) was amplified
360 from Col-0 gDNA, and the *MpSETA* CDS was amplified from cDNA derived from Tak-
361 1 antheridiophores. *proAtSPCH* and *MpSETA* CDS fragments were fused by PCR using
362 PrimeSTAR GXL polymerase (Takara Bio), and the resultant PCR fragment was
363 subcloned into pENTR1A entry clones (Invitrogen) at the SalI and EcoRV restriction sites
364 using In-Fusion HD Cloning Kit (Takara Bio) and transferred into the destination vector
365 pGWB501⁵⁷ using Gateway LR Clonase II Enzyme mix (Thermo Fisher Scientific).
366 *proAtMUTE:MpSETA* and *proAtFAMA:MpSETA* constructs were generated by LR
367 recombination of the R4pGWB501⁵⁸ or R4pGWB601⁵⁸ with a pENTR1A containing the
368 *MpSETA* CDS at the EcoRI sites and either pENTR5'/TOPO_ *proAtMUTE* harboring
369 *proAtMUTE*, 1,930 bp upstream of the translational initiation site, or
370 pENTR5'/TOPO_ *proAtFAMA* harboring *proAtFAMA*, 3,105 bp upstream of the
371 translational initiation site (R4pGWB501_ *proAtMUTE:MpSETA* and

372 R4pGWB601_proAtFAMA:MpSETA). To construct *proAtICE1:MpICE1* or
373 *proAtICE1:MpICE2*, firstly the *AtICE1* promoter (2,578 bp upstream of the translational
374 initiation site) was amplified from Col-0 gDNA, and *MpICE1* or *MpICE2* CDS was
375 amplified from cDNA derived from Tak-1 thalli. *proAtICE1* and *MpICE1* or *MpICE2* CDS
376 fragments were fused by PCR using PrimeSTAR GXL polymerase, and the resultant PCR
377 fragment was subcloned into pENTR1A entry clones at the Sall and EcoRI restriction
378 sites using an In-Fusion HD Cloning Kit and transferred into the destination vector
379 pGWB501⁵⁷ using Gateway LR Clonase II Enzyme mix. The resultant plasmids were
380 introduced into *spch-3/+*, *mute-2/+*, *fama-1/+*, or *ice1-2/+ scrm2-1* heterozygous plants
381 by the previously described method⁵⁹ using *Agrobacterium tumefaciens* strain GV3101.
382 We confirmed that all transformants had a single insertion event by segregation analyses.
383 We used T₃ or T₄ homozygous plants. For *MpICE2* overexpression analyses, the *MpICE2*
384 CDS was transferred into the destination vector pFAST-R02⁶⁰ using Gateway Clonase II
385 Enzyme mix, and the resultant plasmid was introduced into Ws-4, *mute-2/+*, and
386 *proAtMUTE:MpSETA mute-2/+* (#8-4 and #10-11). T₁ seeds expressing TagRFP were
387 selected, and T₁ plants were used to the analyses. We stained the cotyledons by FM4-64
388 and observed them using an LSM780 laser scanning microscope (Carl Zeiss). Images
389 were processed with Fiji (NIH). The sequences of primers used in this study are shown
390 in Supplementary Tables 1 and 2.

391

392 **Gene expression analysis**

393 Publicly available transcriptome data were downloaded from the Sequence Read Archive
394 (SRA) repository. Accession numbers include: sporelings (SRR4450254, SRR4450255,
395 SRR4450256)⁴, male thalli (DRR118949, DRR118950, DRR118951)²⁰, female thalli
396 (DRR118943, DRR118944, DRR118945)²⁰, antheridiophores (DRR050346,
397 DRR050347, DRR050348)²¹, archegoniophores (DRR050351, DRR050352,
398 DRR050353)²¹, antheridia (DRR050349, DRR050350)²¹, archegonia (DRR209029,
399 DRR209030, DRR209031, DRR209031)²², 13 DPF sporophytes (SRR1553297,
400 SRR1553298, SRR1553299)¹⁹, mature sporophytes (SRR896223)⁴. RNA-seq data were
401 preprocessed to filter out low-quality sequences using fastp⁶¹ v.0.20.0. The sequence
402 reads were mapped to the *M. polymorpha* genome v.6.1 (<https://marchantia.info>) by
403 STAR⁶² v.2.7.8a with default parameters. The post-processing of SAM/BAM files was
404 performed using SAMtools⁶³ v.1.11. The read counts for each gene were used to calculate
405 transcript per million (TPM) by using RSEM⁶⁴ v.1.3.0 with default parameters. Plots were
406 created using Rstudio v.1.4.1106 (<https://www.rstudio.com/>).

407

408 **Histology**

409 Sporophytes (stage I and II) were stained with 4',6-diamidino-2-phenylindol (DAPI) as
410 described previously²² and were observed using an LSM780 laser scanning microscope.

411 Plant samples were fixed with 2% (w/v) paraformaldehyde and 2% (v/v)
412 glutaraldehyde in 0.05 M cacodylate buffer (pH 7.4) for 2 hours at room temperature,
413 post-fixed with 2% (v/v) osmium tetroxide in 0.1 M cacodylate buffer for 2 hours at room
414 temperature, dehydrated in an ethanol series, substituted with acetone, and then embedded
415 in Spurr's resin (Polysciences). The Spurr's blocks were cut into semi-thin sections (0.75-
416 2 μm) with glass knives on an ultramicrotome Leica Ultracut UCT (Leica Microsystems)
417 and stained with a solution containing 1% (w/v) sodium tetra-borate and 1% (w/v)
418 toluidine blue O. Sections were mounted on MAS-coated glass slides (Matsunami Glass).

419 Images were obtained using a VB-7010 (KEYENCE)/AxioCam HRc (Zeiss) and were
420 processed with Fiji or Adobe Photoshop Elements 9 (Adobe Systems).

421

422 **Histochemical GUS staining**

423 To construct *proMpSETA::GUS*, we amplified the genomic fragment of the 4,194 bp
424 upstream region of the translational initiation site from Tak-1 gDNA using PrimeSTAR
425 Max DNA polymerase (Takara Bio), subcloned it into pENTR1A at the EcoRI restriction
426 sites using an In-Fusion HD Cloning Kit and then transferred it into the destination vector
427 pMpGWB104⁶⁵ using Gateway LR Clonase II Enzyme mix (Thermo Fisher Scientific).
428 To construct *proMpICE2::Citrine-GUS-NLS*, firstly we amplified the genomic fragment
429 containing the 3,060 bp upstream region of the translational initiation site from Tak-1
430 gDNA, *Citrine* ORF from pMpGWB107⁶⁵, and *GUS-NLS* ORF from pPZP211_35S-NG-
431 GUS-NLS-nosT⁶⁶. These fragments were fused by PCR, subcloned into pENTR1A at the
432 Sall and EcoRV sites using an In-Fusion HD Cloning Kit, and transferred into
433 pMpGWB101⁶⁵. The resultant plasmids were introduced into Tak-1 accession by the
434 previously described method⁶⁷ using *A. tumefaciens* strain GV2260.

435 The tissues of *proMpSETA::GUS* or *proMpICE2::Citrine-GUS-NLS* plants were
436 vacuum-infiltrated and incubated at 37°C overnight in GUS staining solution containing
437 10 mM EDTA (pH 8.0), 100 mM NaH₂PO₄ (pH 7.0), 0.1% (v/v) Triton X-100, 0.5 g
438 L⁻¹ 5-bromo-4-chloro-3-indolyl-β-D-glucuronic acid (X-Gluc), 5 mM potassium-
439 ferrocyanide, and 5 mM potassium-ferricyanide. Samples were washed in 70% (v/v)
440 ethanol and cleared with chloral-hydrate / glycerol solution.

441

442 **Generation of *Mpseta*^{ko} mutants**

443 Tak-1 genomic sequences of 3,125 bp upstream and 3,101 bp downstream of MpSETA
444 bHLH domain coding region were amplified by PCR with a PrimeSTAR Max DNA
445 polymerase and inserted into PacI and AscI sites of pJHY-TMp1²⁸, respectively. The
446 vector was introduced into germinating F₁ spores from Tak-1 and Tak-2 cross via *A.*
447 *tumefaciens* strain GV2260 as previously described⁶⁸. The transformed T₁ plants carrying
448 the targeted insertion were selected by PCR using GoTaq DNA polymerase (Promega).
449 As T₁ plants of *Mpseta-1*^{ko} and *Mpseta-2*^{ko} were both females, male mutants were
450 obtained from F₁ sporelings by crossing female mutants with Tak-1.

451

452 **Reverse transcription PCR**

453 For gene expression analysis, 21 DPF sporophytes were collected from wild type,
454 *Mpseta-1*^{ko}, and *Mpseta-2*^{ko}, and total RNA was extracted by RNeasy Plant Mini Kit
455 (Qiagen) according to the manufacturer's protocol. The quality and quantity of total RNA
456 were evaluated with a NanoDrop 2000 spectrophotometer (Thermo Fisher Scientific).
457 First-strand cDNA was synthesized using ReverTra Ace qPCR RT Master Mix with
458 gDNA Remover (Toyobo), and semiquantitative RT-PCR was undertaken using *MpEF1α*
459 as a loading control⁶⁹.

460

461 **Yeast two-hybrid assay**

462 The coding sequences of MpSETA and MpICE2 were amplified from cDNA derived
463 from mRNA of Tak-1 thalli by PCR using PrimeSTAR Max DNA polymerase or
464 PrimeSTAR GXL polymerase (Takara Bio). The coding sequences of AtICE1 and
465 AtSCRM2 were amplified from cDNA derived from Col-0 leaves using PrimeSTAR

466 GXL polymerase. The resultant PCR fragments were subcloned into pENTR1A at the
467 EcoRI sites or Sall and EcoRV sites using an In-Fusion HD Cloning Kit. To generate a
468 bait destination vector, pDEST-GBKT7-Amp^r, *Amp^r* was amplified from pDEST-
469 GADT7⁷⁰ by PCR using PrimeSTAR Max DNA polymerase, and the fragment was
470 cloned into the SfoI site of pDEST-GBKT7⁷⁰. The inserted fragments, MpSETA,
471 MpICE2, AtICE1, and AtSCRM2 were transferred into pDEST-GADT7 and/or pDEST-
472 GBKT7-Amp^r using Gateway LR Clonase II Enzyme mix. Bait and prey constructs were
473 co-transformed into the yeast strain Y2HGGold (Clontech) using the Frozen-EZ Yeast
474 Transformation II Kit (Zymo Research) and the transformants were grown on solid SD
475 media lacking Leu and Trp (SD-LW). To examine the interaction between the bait and
476 prey proteins, transformants were grown on solid SD media lacking Leu, Trp, His, and
477 adenine with 40 mg L⁻¹ X- α -gal and 200 μ g L⁻¹ Aureobasidin A (SD-LWHA/X/AbA) at
478 30°C. pDEST-GBKT7-Amp^r and pDEST-GADT7 were used as negative controls
479 (empty).

480

481 **BiFC**

482 The coding sequences of MpSETA, MpICE2, AtICE1 and AtSCRM2 subcloned into
483 pENTR1A described above were transferred into the pB4GWnY and/or
484 pB4GWcY/pB4cYGW binary vector⁷¹ using LR reaction to be fused with N-terminal or
485 C-terminal half of YFP (MpSETA-*nYFP*, MpICE2-*cYFP*, *cYFP*-AtICE1, and *cYFP*-
486 AtSCRM2 driven by the *CaMV35S* promoter). Transformed *A. tumefaciens* strain
487 GV3101 cells harboring expression vectors were cultured and resuspended in distilled
488 water to a final optical density of OD₆₀₀ = 1.0. Mixed *Agrobacterium* cultures were
489 infiltrated into 4-week-old *Nicotiana benthamiana* leaves. Nuclei were stained with DAPI
490 at the 1 mg L⁻¹ concentration for 30 min. Samples were observed 1.5 days post-
491 inoculation (DPI) by an LSM780 laser scanning microscope. pB4GWnY and
492 pB4GWcY/pB4cYGW were used as a negative control (empty).

493

494 **Generation of *Mpice2*^{ge} mutants**

495 To generate *Mpice2*^{ge} mutants, the MpICE2 locus encoding the bHLH domain was edited
496 using CRISPR/Cas9 based genome-editing system as previously described³¹. Two sgRNA
497 were designed to generate *Mpice2*^{ge} mutants. The oligonucleotides encoding sgRNA were
498 cloned into pMpGE_En03³¹ between BsaI sites and then introduced into pMpGE010³¹.
499 Male and female mutants that do not harbor T-DNA containing *Cas9* were obtained from
500 F₁ sporelings crossed with wild type and *Mpice2-2*^{ge} or *Mpice2-6*^{ge}.

501

502 **Complementation tests of *Mpseta*^{ko} and *Mpice2*^{ge}**

503 To construct gMpSETA for *Mpseta-1*^{ko} complementation, the genomic region containing
504 the 4,194 bp upstream region and coding sequences was amplified from Tak-1 genomic
505 DNA. The fragment was cloned into pENTR1A between EcoRI sites and then introduced
506 into pMpGWB301⁶⁵. The resultant plasmids were introduced into female *Mpseta-1*^{ko}.
507 Male gMpSETA *Mpseta-1*^{ko} was obtained from F₁ sporelings produced from crosses
508 between female gMpSETA *Mpseta-1*^{ko} and male *Mpseta-1*^{ko}. To construct gMpICE2 for
509 *Mpice2-6*^{ge}, the genomic region containing 3,060 bp upstream regions and coding
510 sequences was amplified from Tak-1 genomic DNA. The fragment was cloned into
511 pENTR1A between Sall and EcoRV sites and then introduced into pMpGWB101⁶⁵. The
512 resultant plasmids were introduced into female *Mpice2-6*^{ge}. A male gMpICE2 *Mpice2-*

513 6^{ge} was obtained from a F₁ sporeling derived from a cross between a female gMpICE2
514 Mpice2-6^{ge} and a male Mpice2-6^{ge}.

515

516

517 References

- 518 1. Ligrone, R., Duckett, J. G. & Renzaglia, K. S. Major transitions in the evolution of
519 early land plants: A bryological perspective. *Ann. Bot.* **109**, 851–871 (2012).
- 520 2. Romani, F. & Moreno, J. E. Molecular mechanisms involved in functional
521 macroevolution of plant transcription factors. *New Phytol.* **230**, 1345–1353 (2021).
- 522 3. Catarino, B., Hetherington, A. J., Emms, D. M., Kelly, S. & Dolan, L. The stepwise
523 increase in the number of transcription factor families in the precambrian predated
524 the diversification of plants on land. *Mol. Biol. Evol.* **33**, 2815–2819 (2016).
- 525 4. Bowman, J. L. *et al.* Insights into land plant evolution garnered from the
526 *Marchantia polymorpha* genome. *Cell* **171**, 287-304.e15 (2017).
- 527 5. Pires, N. & Dolan, L. Origin and Diversification of Basic-Helix-Loop-Helix
528 Proteins in Plants. *Mol. Biol. Evol.* **5**, 911–912 (2010).
- 529 6. MacAlister, C. A., Ohashi-Ito, K. & Bergmann, D. C. Transcription factor control
530 of asymmetric cell divisions that establish the stomatal lineage. *Nature* **445**, 537–
531 540 (2007).
- 532 7. Pillitteri, L. J., Sloan, D. B., Bogenschutz, N. L. & Torii, K. U. Termination of
533 asymmetric cell division and differentiation of stomata. *Nature* **445**, 501–505
534 (2007).
- 535 8. Ohashi-Ito, K. & Bergmann, D. C. *Arabidopsis* FAMA controls the final
536 proliferation/differentiation switch during stomatal development. *Plant Cell* **18**,
537 2493–2505 (2006).
- 538 9. Kanaoka, M. M. *et al.* SCREAM/ICE1 and SCREAM2 specify three cell-state
539 transitional steps leading to *Arabidopsis* stomatal differentiation. *Plant Cell* **20**,
540 1775–1785 (2008).
- 541 10. Chater, C. C. *et al.* Origin and function of stomata in the moss *Physcomitrella*
542 *patens*. *Nat. Plants* **2**, 16179 (2016).
- 543 11. Caine, R. S. *et al.* Stomata and sporophytes of the model moss *Physcomitrium*
544 *patens*. *Front. Plant Sci.* **11**, 643 (2020).
- 545 12. Chater, C. C. C., Caine, R. S., Fleming, A. J. & Gray, J. E. Origins and evolution
546 of stomatal development. *Plant Physiol.* **174**, 624–638 (2017).
- 547 13. Harris, B. J. *et al.* Phylogenomic evidence for the monophyly of bryophytes and
548 the reductive evolution of stomata. *Curr. Biol.* **30**, 2001-2012.e2 (2020).
- 549 14. Flores-Sandoval, E., Romani, F. & Bowman, J. L. Co-expression and
550 transcriptome analysis of *Marchantia polymorpha* transcription factors supports
551 class C ARFs as independent actors of an ancient auxin regulatory module. *Front.*
552 *Plant Sci.* **9**, 1345 (2018).
- 553 15. Feller, A., Hernandez, J. M. & Grotewold, E. An ACT-like domain participates in
554 the dimerization of several plant basic-helix-loop-helix transcription factors. *J.*
555 *Biol. Chem.* **281**, 28964–28974 (2006).
- 556 16. Seo, H. *et al.* Intragenic suppressors unravel the role of the SCREAM ACT-like
557 domain for bHLH partner selectivity in stomatal development. *Proc. Natl. Acad.*
558 *Sci. U. S. A.* **119**, e2117774119 (2022).
- 559 17. Linde, A. M., Eklund, D. M., Cronberg, N., Bowman, J. L. & Lagercrantz, U. Rates

- 560 and patterns of molecular evolution in bryophyte genomes, with focus on complex
561 thalloid liverworts, Marchantiopsida. *Mol. Phylogenet. Evol.* **165**, 107295 (2021).
- 562 18. Pillitteri, L. J., Bogenschutz, N. L. & Torii, K. U. The bHLH protein, MUTE,
563 controls differentiation of stomata and the hydathode pore in *Arabidopsis*. *Plant*
564 *Cell Physiol.* **49**, 934–943 (2008).
- 565 19. Frank, M. H. & Scanlon, M. J. Transcriptomic evidence for the evolution of shoot
566 meristem function in sporophyte-dominant land plants through concerted selection
567 of ancestral gametophytic and sporophytic genetic programs. *Mol. Biol. Evol.* **32**,
568 355–367 (2015).
- 569 20. Yamaoka, S. *et al.* Generative cell specification requires transcription factors
570 evolutionarily conserved in land plants. *Curr. Biol.* **28**, 479–486.e5 (2018).
- 571 21. Higo, A. *et al.* Transcriptional framework of male gametogenesis in the liverwort
572 *Marchantia polymorpha* L. *Plant Cell Physiol.* **57**, 325–338 (2016).
- 573 22. Hisanaga, T. *et al.* Deep evolutionary origin of gamete-directed zygote activation
574 by KNOX/BELL transcription factors in green plants. *Elife* **10**, e57090 (2021).
- 575 23. Shimamura, M. *Marchantia polymorpha*: Taxonomy, phylogeny and morphology
576 of a model system. *Plant Cell Physiol.* **57**, 230–256 (2016).
- 577 24. Haig, D. Filial mistletoes: The functional morphology of moss sporophytes. *Ann.*
578 *Bot.* **111**, 337–345 (2013).
- 579 25. Ligrone, R., Duckett, J. G. & Renzaglia, K. S. The origin of the sporophyte shoot
580 in land plants: A bryological perspective. *Ann. Bot.* **110**, 935–941 (2012).
- 581 26. Durand, E. J. The development of the sexual organs and sporogonium of
582 *Marchantia polymorpha*. *Bull. Torrey Bot. Club* **7**, 321–335 (1908).
- 583 27. Hernández-García, J. *et al.* Coordination between growth and stress responses by
584 DELLA in the liverwort *Marchantia polymorpha*. *Curr. Biol.* **31**, 3678–3686.e11
585 (2021).
- 586 28. Ishizaki, K., Johzuka-Hisatomi, Y., Ishida, S., Iida, S. & Kohchi, T. Homologous
587 recombination-mediated gene targeting in the liverwort *Marchantia polymorpha*
588 L. *Sci. Rep.* **3**, 1532 (2013).
- 589 29. Shaw, J. & Renzaglia, K. Phylogeny and diversification of bryophytes. *Am. J. Bot.*
590 **91**, 1557–1581 (2004).
- 591 30. Wu, Z. *et al.* Multiple transcriptional factors control stomata development in rice.
592 *New Phytol.* **223**, 220–232 (2019).
- 593 31. Sugano, S. S. *et al.* Efficient CRISPR/Cas9-based genome editing and its
594 application to conditional genetic analysis in *Marchantia polymorpha*. *PLoS One*
595 **13**, e0205117 (2018).
- 596 32. Sugano, S. S. *et al.* CRISPR/Cas9-mediated targeted mutagenesis in the liverwort
597 *Marchantia polymorpha* L. *Plant Cell Physiol.* **55**, 475–481 (2014).
- 598 33. Chinnusamy, V. *et al.* ICE1: A regulator of cold-induced transcriptome and
599 freezing tolerance in *Arabidopsis*. *Genes Dev.* **17**, 1043–1054 (2003).
- 600 34. Davies, K. A. & Bergmann, D. C. Functional specialization of stomatal bHLHs
601 through modification of DNA-binding and phosphoregulation potential. *Proc. Natl.*
602 *Acad. Sci. U. S. A.* **111**, 15585–15590 (2014).
- 603 35. MacAlister, C. A. & Bergmann, D. C. Sequence and function of basic helix-loop-
604 helix proteins required for stomatal development in *Arabidopsis* are deeply
605 conserved in land plants. *Evol. Dev.* **13**, 182–192 (2011).
- 606 36. Merced, A. & Renzaglia, K. S. Structure, function and evolution of stomata from

- 607 a bryological perspective. *Bryophyt. Divers. Evol.* **39**, 7–20 (2017).
- 608 37. Wei, D. *et al.* INDUCER OF CBF EXPRESSION 1 is a male fertility regulator
609 impacting anther dehydration in *Arabidopsis*. *PLoS Genet.* **14**, e1007695 (2018).
- 610 38. Higo, A. *et al.* Transcription factor DUO1 generated by neo-functionalization is
611 associated with evolution of sperm differentiation in plants. *Nat. Commun.* **9**, 5283
612 (2018).
- 613 39. Menand, B. *et al.* An ancient mechanism controls the development of cells with a
614 rooting function in land plants. *Science* **316**, 1477–1480 (2007).
- 615 40. Koshimizu, S. *et al.* *Physcomitrella* MADS-box genes regulate water supply and
616 sperm movement for fertilization. *Nat. Plants* **4**, 36–45 (2018).
- 617 41. Shirakawa, M. *et al.* FAMA is an essential component for the differentiation of
618 two distinct cell types, myrosin cells and guard cells, in *Arabidopsis*. *Plant Cell* **26**,
619 4039–4052 (2014).
- 620 42. Yasui, Y. *et al.* GEMMA CUP-ASSOCIATED MYB1, an ortholog of axillary
621 meristem regulators, is essential in vegetative reproduction in *Marchantia*
622 *polymorpha*. *Curr. Biol.* **29**, 3987–3995.e5 (2019).
- 623 43. Proust, H. *et al.* RSL class I genes controlled the development of epidermal
624 structures in the common ancestor of land plants. *Curr. Biol.* **26**, 93–99 (2016).
- 625 44. Puttick, M. N. *et al.* The interrelationships of land plants and the nature of the
626 ancestral embryophyte. *Curr. Biol.* **28**, 733–745.e2 (2018).
- 627 45. Renzaglia, K. & Garbary, D. J. Motile gametes of land plants: Diversity,
628 development, and evolution. *CRC. Crit. Rev. Plant Sci.* **20**, 107–213 (2001).
- 629 46. Sakakibara, K., Nishiyama, T., Deguchi, H. & Hasebe, M. Class 1 KNOX genes
630 are not involved in shoot development in the moss *Physcomitrella patens* but do
631 function in sporophyte development. *Evol. Dev.* **10**, 555–566 (2008).
- 632 47. Coudert, Y., Novák, O. & Harrison, C. J. A KNOX-cytokinin regulatory module
633 predates the origin of indeterminate vascular plants. *Curr. Biol.* **29**, 2743–2750.e5
634 (2019).
- 635 48. Li, M. & Sack, F. D. Myrosin idioblast cell fate and development are regulated by
636 the *Arabidopsis* transcription factor FAMA, the auxin pathway, and vesicular
637 trafficking. *Plant Cell* **26**, 4053–4066 (2014).
- 638 49. Shirakawa, M., Tanida, M. & Ito, T. The cell differentiation of idioblast myrosin
639 cells: Similarities with vascular and guard cells. *Front. Plant Sci.* **12**, 829541
640 (2021).
- 641 50. Li, F. W. *et al.* *Anthoceros* genomes illuminate the origin of land plants and the
642 unique biology of hornworts. *Nat. Plants* **6**, 259–272 (2020).
- 643 51. Han, S. *et al.* MUTE directly orchestrates cell-state switch and the single
644 symmetric division to create stomata. *Dev. Cell* **45**, 303–315.e5 (2018).
- 645 52. Lau, O. S. *et al.* Direct roles of SPEECHLESS in the specification of stomatal self-
646 renewing cells. *Science* **345**, 1605–1609 (2014).
- 647 53. Leebens-Mack, J. H. *et al.* One thousand plant transcriptomes and the
648 phylogenomics of green plants. *Nature* **574**, 679–685 (2019).
- 649 54. Katoh, K. & Toh, H. Recent developments in the MAFFT multiple sequence
650 alignment program. *Brief. Bioinform.* **9**, 286–298 (2008).
- 651 55. Waterhouse, A. M., Procter, J. B., Martin, D. M. A., Clamp, M. & Barton, G. J.
652 Jalview Version 2-A multiple sequence alignment editor and analysis workbench.
653 *Bioinformatics* **25**, 1189–1191 (2009).

- 654 56. Kumar, S., Stecher, G. & Tamura, K. MEGA7: Molecular Evolutionary Genetics
655 Analysis version 7.0 for bigger datasets. *Mol. Biol. Evol.* **33**, 1870–1874 (2016).
- 656 57. Nakagawa, T. *et al.* Improved gateway binary vectors: High-performance vectors
657 for creation of fusion constructs in transgenic analysis of plants. *Biosci. Biotechnol.*
658 *Biochem.* **71**, 2095–2100 (2007).
- 659 58. Nakamura, S. *et al.* Gateway binary vectors with the bialaphos resistance gene, bar,
660 as a selection marker for plant transformation. *Biosci. Biotechnol. Biochem.* **74**,
661 1315–1319 (2010).
- 662 59. Clough, S. J. & Bent, A. F. Floral dip: A simplified method for *Agrobacterium*-
663 mediated transformation of *Arabidopsis thaliana*. *Plant J.* **16**, 735–743 (1998).
- 664 60. Shimada, T. L., Shimada, T. & Hara-Nishimura, I. A rapid and non-destructive
665 screenable marker, FAST, for identifying transformed seeds of *Arabidopsis*
666 *thaliana*. *Plant J.* **61**, 519–528 (2010).
- 667 61. Chen, S., Zhou, Y., Chen, Y. & Gu, J. Fastp: An ultra-fast all-in-one FASTQ
668 preprocessor. *Bioinformatics* **34**, i884–i890 (2018).
- 669 62. Dobin, A. *et al.* STAR: Ultrafast universal RNA-seq aligner. *Bioinformatics* **29**,
670 15–21 (2013).
- 671 63. Li, H. *et al.* The Sequence Alignment/Map format and SAMtools. *Bioinformatics*
672 **25**, 2078–2079 (2009).
- 673 64. Li, B. & Dewey, C. N. RSEM: accurate transcript quantification from RNA-Seq
674 data with or without a reference genome. *BMC Bioinformatics* **12**, 323 (2011).
- 675 65. Ishizaki, K. *et al.* Development of gateway binary vector series with four different
676 selection markers for the liverwort *Marchantia polymorpha*. *PLoS One* **10**,
677 e0138876 (2015).
- 678 66. Matsushita, T., Mochizuki, N. & Nagatani, A. Dimers of the N-terminal domain of
679 phytochrome B are functional in the nucleus. *Nature* **424**, 571–574 (2003).
- 680 67. Tsuboyama, S., Nona, S., Ezura, H. & Kodama, Y. Improved G-AgarTrap : A
681 highly efficient transformation method for intact gemmalings of the liverwort
682 *Marchantia polymorpha*. *Sci. Rep.* **8**, 10800 (2018).
- 683 68. Ishizaki, K., Chiyoda, S., Yamato, K. T. & Kohchi, T. *Agrobacterium*-mediated
684 transformation of the haploid liverwort *Marchantia polymorpha* L., an emerging
685 model for plant biology. *Plant Cell Physiol.* **49**, 1084–1091 (2008).
- 686 69. Rövekamp, M., Bowman, J. L. & Grossniklaus, U. *Marchantia* MpRKD regulates
687 the gametophyte-sporophyte transition by keeping egg cells quiescent in the
688 absence of fertilization. *Curr. Biol.* **26**, 1782–1789 (2016).
- 689 70. Rossignol, P., Collier, S., Bush, M., Shaw, P. & Doonan, J. H. *Arabidopsis* POT1A
690 interacts with TERT-V(18), an N-terminal splicing variant of telomerase. *J. Cell*
691 *Sci.* **120**, 3678–3687 (2007).
- 692 71. Hino, T. *et al.* Two Sec13p homologs, AtSec13A and AtSec13B, redundantly
693 contribute to the formation of COPII transport vesicles in *Arabidopsis thaliana*.
694 *Biosci. Biotechnol. Biochem.* **75**, 1848–1852 (2011).

695

696 Acknowledgements

697 We thank Tsuyoshi Nakagawa (Shimane University, Japan), Shoji Mano (National
698 Institute for Basic Biology, Japan), Shigeo S. Sugano (National Institute of Advanced
699 Industrial Science and Technology, Japan), and Keiko U. Torii (The University of Texas
700 at Austin, USA) for sharing the materials. We also thank Keiji Nakajima (Nara Institute

701 of Science and Technology, Japan) for sharing the figures of plants in Fig. 5b. We are
702 grateful to James Raymond for critical readings of this manuscript. This work was
703 supported by MEXT/JSPS KAKENHI grants to M.S. (JP19K06722 and JP20H05416),
704 to K.T. (JP26711017 and JP18K06283), to Y.O. (JP18K19964), to T.M. (JP20H05905
705 and JP20H05906), to I.H.-N. (JP15H05776), to R.N. (JP20H04884) and to T.S.
706 (JP18K06284); Grants-in-Aid JSPS Fellows to K.C.M. (JP21J14990) and to M.S.
707 (JP12J05453) and; the Takeda Science Foundation, the Kato Memorial Bioscience
708 Foundation, and the Ohsumi Frontier Science Foundation to M.S. J.L.-M. and Y-T Lu
709 were supported by Ph.D. studentships from the Darwin Trust of Edinburgh.

710

711 **Author contributions**

712 K.C.M. and T.S. conceived and designed the research in general; K.C.M. performed most
713 of the experiments and analyzed the data; M.S. and Y.M. performed the experiments on
714 *MpSETA*; J.L.-M., Y.-T. L., G.I., and J.G. performed the experiments on *MpICE2*; K.T.,
715 Y.O., T.M., I.H.-N., R.N., J.G., and T.K. supervised the experiments; K.C.M. and T.S.
716 wrote the manuscript; All authors read, edited, and approved the manuscript.

717

718 **Competing interests**

719 The authors declare no competing interests.

720

721 **Figure legends**

722 **Fig. 1 | MpSETA is the only bHLH transcription factor that belongs to subfamily Ia**
723 **in *M. polymorpha*.** **a**, A maximum-likelihood bHLH phylogenetic tree of subfamilies Ia,
724 Ib(1) (purple), II (gray), and III(a+c) (outgroup) is shown. Numbers at branches indicate
725 bootstrap values calculated from 1,000 replicates. Ia bHLHs are divided into four groups:
726 TEC1/6 clade (light blue), MYC70 clade (cream-yellow), SMF/FAMA clade (magenta),
727 and SPCH/MUTE clade (green). Species are abbreviated as follows: Mp, *M. polymorpha*
728 (liverwort); Lc, *L. cruciata* (liverwort); Pp, *P. patens* (moss); Cepur, *Ceratodon purpureus*
729 (moss); Aagr, *Anthoceros agrestis* (hornwort); Sm, *Selaginella moellendorffii*
730 (lycophyte); AmTr, *Amborella trichopoda* (basal angiosperm); Os, *Oryza sativa*
731 (monocot); At, *A. thaliana* (dicot). An arrow indicates MpSETA/MpBHLH35
732 (Mp2g04160), and arrowheads indicate bHLH TFs mentioned as FAMA-like bHLH TFs
733 in a previous study¹⁴. Amino acid sequences from only *A. thaliana* and *M. polymorpha*
734 were used for subfamilies Ib(1), II, and III(a+c). **b**, Confocal images of *A. thaliana* abaxial
735 cotyledons of wild type (Ws-4), *mute-2*, and *proAtMUTE:MpSETA mute-2* at 9 days after
736 stratification (DAS). The upper panels and lower panels show the middle area and tip area
737 of the cotyledons, respectively (left image). Arrowheads and asterisks indicate stomata
738 and hydathode pores, respectively. Bars, 100 μ m (**b**, confocal images), and 1 mm (**b**, left).
739

740 **Fig. 2 | MpSETA is preferentially expressed in developing sporophyte.** **a**, Box plot
741 showing the expression profiles of MpSETA across nine *M. polymorpha* tissues. Y-axis
742 shows transcripts per million (TPM). Sporeling and thalli are vegetative gametophytic (*n*)
743 organs. Antheridiophores and archegoniophores are haploid male and female
744 reproductive receptacles, respectively. Antheridia and archegonia are the organs that
745 produce sperms and egg cells, respectively. Sporophytes are diploid (*2n*) organs
746 developed after fertilization. **b**, Tissue section of mature *M. polymorpha* sporophyte
747 (stage IX). **c**, Developmental stages of *M. polymorpha* sporophytes after 4–40 days'
748 postfertilization. (I) sporophyte differentiating an epibasal cell and a hypobasal cell, (II)
749 4-cell or 8-cell sporophyte, (III) sporophyte differentiating amphithecium and
750 endothecium, (IV) later globular sporophyte, (V) sporophyte differentiating foot, seta,
751 and archesporial tissues, (VI) sporophyte differentiating sporogenous cells and
752 elaterocytes (or elater mother cell), (VII) sporophyte differentiating sporocytes (or spore
753 mother cells), (VIII) sporophyte differentiating spore tetrads after meiosis, (IX) mature
754 sporophyte before the seta elongation, (X) mature sporophyte after seta elongation.
755 Arrows indicate the endothecium. Arrowheads indicate the cell wall of the first cell
756 division. **d**, Magnified images showing the foot and seta for each stage of wild-type
757 sporophytes. Same images as used in (c). **e**, The formation of the cell files of seta in the
758 wild type stage VIII sporophyte. Enlarged images of the square areas are shown in (d).
759 Arrowheads indicate the plane of proliferative cell divisions. **f**, Histochemical detection
760 of β -glucuronidase (GUS) activity in the sporophytes crossed with male wild type and
761 female *proMpCYCB;1:Dbox-GUS*. **g**, Histochemical detection of β -glucuronidase (GUS)
762 activity driven by MpSETA promoter in the developing seta region from stage IV to stage
763 IX. f, foot; s, seta; at, archesporial tissue; sp, sporangium; ca, calyptra; p, pseudoperianth.
764 Arrowheads indicate the cell wall of the first cell division. Bars, 50 μ m (**c**, top), and 100
765 μ m (**b**, **c**, bottom, **d**, **f** and **g**).
766

767 **Fig. 3 | *Mpseta*^{ko} mutants show developmental defects in the seta. a,b**, Longitudinal
768 sections of sporophytes of indicated genotypes. Enlarged images of the square areas are
769 shown in (b). Dashed and solid arrows indicate the length of the sporophyte (SP) and the
770 length from the boundary between gametophyte and sporophyte to the proximal side of
771 sporangium (SF), respectively. **c,d**, Quantitative data showing the SF/SP length ratio and
772 the number of cells in the seta region. Since the boundary between seta and foot is unclear,
773 cells excluding transfer cells (the cells at the boundary between gametophyte and
774 sporophyte) were used to count the number of cells. The different letters indicate
775 significantly different mean values at $p < 0.01$ (Tukey's HSD test). ($n = 6$ independent
776 lines). **e**, Comparative analyses of the tissue development between wild type and *Mpseta*-
777 *l*^{ko}. Enlarged images of longitudinal sections of stage VI, stage VII, and stage VIII
778 sporophytes. **f**, Sporogenesis process in wild type and *Mpseta*-*l*^{ko}. Sporocytes are the cells
779 before the pre-meiotic stage, and spore tetrads are the cells immediately after meiosis. **g**,
780 One month-post-fertilization archegoniophores that produce mature sporophytes.
781 Arrowheads indicate sporangia exposed to the outside of calyptra due to elongation of
782 seta cells. Bars, 50 μm (f), 100 μm (a, b, e), and 5 mm (e).

783
784 **Fig. 4 | *MpICE2* regulates setal development in cooperation with *MpSETA*. a**. Box
785 plot showing the expression profiles of *MpICE1* and *MpICE2* across nine *M. polymorpha*
786 tissues. Y-axis shows transcripts per million (TPM). **b**, Y2H assays showing the
787 interaction between *MpSETA* and *MpICE2*. *MpSETA* fused with GAL4 DNA-binding
788 domain (DBD) was used as bait, while *MpICE2* fused with GAL4 activation domain
789 (AD) was used as prey. DBD alone and AD alone were used as the negative control. **c**,
790 BiFC assays showing the interaction between *MpSETA* and *MpICE2* in *N. benthamiana*
791 leaf epidermal cells. *MpSETA* was fused to the N-terminal fragment of EYFP (nYFP),
792 while *MpICE2* was fused to the C-terminal fragment of EYFP (cYFP). nYFP alone and
793 cYFP alone were used as the negative control. Nuclei were stained by 4',6-diamidino-2-
794 phenylindole (DAPI). **d,e**, Longitudinal sections of sporophytes of indicated genotypes.
795 Enlarged images of the square areas are shown in (e). Dashed and solid arrows indicate
796 the length of the sporophyte (SP) and the length from the boundary between gametophyte
797 and sporophyte to the proximal side of sporangium (SF), respectively. **f,g**, Quantitative
798 data showing the SF/SP length ratio and the number of cells in the seta region. Since the
799 boundary between seta and foot is unclear, cells excluding transfer cells (the cells at the
800 boundary between gametophyte and sporophyte) were used to count the number of cells.
801 The different letters indicate significantly different mean values at $p < 0.01$ (Tukey's HSD
802 test) ($n = 6$ or 7 independent lines). **h**, One month-post-fertilization archegoniophores that
803 produce mature sporophytes. Arrowheads indicate sporangia exposed to the outside of
804 calyptra due to elongation of seta cells. Bars, 10 μm (c, YFP, DAPI, and Merge), 100 μm
805 (c, left, d, and e), and 5 mm (f).

806
807 **Fig. 5 | Function and co-option of the Ia-IIIb bHLH module during the evolution of**
808 **land plants. a**, Schematic model comparing the molecular functions of the Ia-IIIb bHLH
809 TF modules in *A. thaliana* and *M. polymorpha* during cell fate determination. In *A.*
810 *thaliana*, the heterodimer of Ia bHLHs (SPCH, MUTE, and FAMA) and IIIb bHLHs
811 (ICE1 and SCRM2) control the development of stomata. In *M. polymorpha*, the
812 heterodimer of Ia bHLH (*MpSETA*) and IIIb bHLH (*MpICE2*) regulates cell
813 differentiation and cell division in the seta precursor transition and might directly or

814 indirectly be involved in the symmetric division of a putative seta mother cell. **b**, An
815 evolutionary model for the Ia-IIIb bHLH TF module. Co-option of the Ia-IIIb bHLH
816 module might have occurred multiple times independently during the evolution of land
817 plants. First, stomata and a transcriptional module consisting of Ia-IIIb bHLHs evolved
818 in the common ancestor of land plants. In the ancestral plant, the Ia bHLHs may have had
819 MUTE- and FAMA-like functions. Second, the Ia-IIIb bHLH TF module might have been
820 co-opted to regulate setal development in the ancestor of the Setophyta. Third, after
821 mosses and liverworts diverged, the common ancestor of liverworts lost its stomata. A co-
822 option of the Ia-IIIb bHLH module occurred in the Brassicales plants for regulating
823 myrosin idioblast development.

824

825 **Extended Data**

826 **Extended Data Fig. 1 | Comparison of the domain architecture of Ia bHLHs in land**

827 **plants. a**, A diagram of the domain architecture of MpSETA (*M. polymorpha*), PpSMF1,
828 PpSMF2 (*P. patens*), AtSPCH, AtMUTE, and AtFAMA (*A. thaliana*). While no PEST
829 domain was identified, MpSETA has a bHLH domain and SMF domain conserved at the
830 C-terminus like other Ia bHLH proteins. SMF domain is structurally considered to be the
831 ACT-like domain, which is a putative domain for protein-protein dimerization. **b**,
832 Sequence alignment of the bHLH domain of Ia bHLH proteins. Ia bHLHs are surrounded
833 by a black box, and others are Ib(1) bHLHs. Asterisks indicate amino acids that are
834 assumed to be important for binding to the E-box (CANNTG), and the triangles indicate
835 amino acids that are assumed to be important for dimerization of the bHLH domain. The
836 yellow box indicates the LxCxE motif, which is a binding motif with Retinoblastoma-
837 related (RBR). **c**, Sequence alignment of the C-terminal SMF domain of Ia bHLH proteins.

838

839 **Extended Data Fig. 2 | Function of MpSETA in A. thaliana Ia bHLH mutants. a**,

840 Confocal images of *A. thaliana* abaxial cotyledons of wild type (Col-0), *spch-3*, and
841 *proAtSPCH:MpSETA spch-3* at 9 days after stratification (DAS). **b**, Confocal images of *A.*
842 *thaliana* abaxial cotyledons of wild type (Col-0), *fama-1*, and *proAtFAMA:MpSETA fama-*
843 *1* at 9 DAS. Brackets and arrows indicate *fama* tumors and stomatal-lineage cells,
844 respectively. **c**, Quantitative data of the distribution of the number of cell divisions that
845 occurred in the stomatal lineage in each genotype. ($n > 320$ cells per genotype, 9 DAS
846 cotyledons). **d**, Y2H assays in which the MpSETA fused with GAL4 DNA-binding
847 domain (DBD) was used as bait, and the AtICE1 and AtSCRM2 fused with GAL4
848 activation domain (AD) were used as prey. DBD alone and AD alone were used as the
849 negative controls. **e**, BiFC assays showing the interaction between MpSETA and AtICE1
850 or AtSCRM2 in *N. benthamiana* leaf epidermal cells. MpSETA was fused to the N-
851 terminal fragment of EYFP (nYFP), while AtICE1 or AtSCRM2 was fused to the C-
852 terminal fragment of EYFP (cYFP). nYFP alone and cYFP alone were used as the
853 negative control. Nuclei were stained by DAPI. Bars, 10 μm (**e**), and 100 μm (**a,b**).

854

855 **Extended Data Fig. 3 | Expression analysis of MpSETA in the gametophytic tissues.**

856 Histochemical detection of β -glucuronidase (GUS) activity driven by MpSETA promoter
857 in the developing antheridia. Bars, 1 mm.

858

859 **Extended Data Fig. 4 | Generation and phenotypes of MpSETA knock-out lines. a**,

860 Structure of the MpSETA locus disrupted by homologous recombination. Knock-out lines

861 have a deletion in the bHLH domain coding region. White boxes indicate the exons of the
862 MpSETA coding sequence. DT-A, diphtheria toxin A fragment gene; *Hgr^R*, hygromycin
863 resistant gene. **b**, Genotyping of the *Mpseta^{ko}* lines used in this study to distinguish the
864 sex. *rbm27*, a male-specific marker; *rhf73*, a female-specific marker. **c**, Genotyping of the
865 *Mpseta^{ko}* lines. The position of primers used for PCR is shown in **(a)**. M, Male; F, Female.
866 **d**, RT-PCR to confirm the loss of the full-length MpSETA transcript in *Mpseta^{ko}* lines in
867 21 DPF sporophytes. MpEF1 α was used as an internal control. **e**, Spermatogenesis
868 process in WT and *Mpseta^{ko}* lines. All images are at the same scale. Bars, 10 μ m (**e**).

869
870 **Extended Data Fig. 5 | Phylogenetic tree of IIIb bHLH TFs.** A maximum-likelihood
871 bHLH phylogenetic tree of subfamilies IIIb, III (a+c) (light blue), and III(d+e) (outgroup)
872 is shown. Numbers at branches indicate bootstrap values calculated from 1,000 replicates.
873 IIIb bHLHs are divided into 2 groups: ICE/SCRM clade (orange) and NFL clade
874 (magenta). Species are abbreviated as follows: Mp, *M. polymorpha* (liverwort); Lc, *L.*
875 *cruciata* (liverwort); Pp, *P. patens* (moss); Cepur, *Ceratodon purpureus* (moss); Agr,
876 *Anthoceros agrestis* (hornwort); Sm, *Selaginella moellendorffii* (lycophyte); AmTr,
877 *Amborella trichopoda* (basal angiosperm); Os, *Oryza sativa* (monocot); At, *A. thaliana*
878 (dicot). Arrows indicate MpICE1 (Mp4g04910) and MpICE2 (Mp4g04920). For the
879 phylogenetic construction of subfamilies III(a+c) and III(d+e), we used the amino acid
880 sequences from only *A. thaliana* and *M. polymorpha*.

881
882 **Extended Data Fig. 6 | Comparison of the domain architecture of IIIb bHLHs in**
883 **land plants.** **a**, A diagram of the domain architecture of MpICE1, MpICE2 (*M.*
884 *polymorpha*), PpSCRM1 (*P. patens*), AtICE1, and AtSCRM2 (*A. thaliana*). MpICE1 and
885 MpICE2 have a bHLH domain and ACT-like domain conserved at the C-terminus like
886 other IIIb bHLH proteins. **b**, Sequence alignment of the bHLH domain of IIIb bHLH
887 proteins. IIIb bHLHs are surrounded by a black box, and others are outgroup. Asterisks
888 indicate amino acids that are assumed to be important for binding to the E-box
889 (CANNTG). **c**, Sequence alignment of the C-terminal ACT-like domain of IIIb bHLH
890 proteins.

891
892 **Extended Data Fig. 7 | The expression analysis of MpICE2.** **a**, Histochemical detection
893 of β -glucuronidase (GUS) activity driven by MpICE2 promoter in the vegetative thallus.
894 **b**, Confocal images of the dorsal epidermis of *proMpICE2:Citrine-GUS-NLS* line. Upper
895 and lower panels indicate the epidermis around the apical notch and the epidermis around
896 the midrib, respectively. Arrows indicate the air pores. **c,d**, Histochemical detection of
897 GUS activity driven by MpICE2 promoter in the gametophytic reproductive organs. An
898 antheridiophore (**c**) and an archegoniophore (**d**) are shown. **e**, Expression pattern of
899 MpICE2 in the developing sporophytes. f, foot; s, seta; at, archesporial tissue; sp,
900 sporangium; ca, calyptra; p, pseudoperianth (*n*). Arrowheads indicate the cell wall of the
901 first cell division. Bars, 5 mm (**c** and **d**), 100 μ m (**b** and **e**).

902
903 **Extended Data Fig. 8 | Generation of Mpice2 mutants by CRISPR/Cas9.** **a**, Schematic
904 representation of the MpICE2 gene and the resulting mutations in the obtained
905 CRISPR/Cas9-generated alleles. Gray, white, and blue boxes indicate the coding
906 sequences (CDS), the untranslated regions (UTR), and the bHLH domain coding region,
907 respectively. **b**, Sequence alignment of putative translational products of wild type and

908 *Mpice2^{ge}* mutants. Asterisks indicate the amino acids that are assumed to be important for
909 binding to E-box.

910

911 **Extended Data Fig. 9 | Functional analysis of MpICE1 and MpICE2 in *A. thaliana***
912 **mutants. a**, Confocal images of *A. thaliana* abaxial cotyledons of wild type (Ws-4), *ice1-*
913 *2 scrm2-1*, and *proAtMUTE:MpSETA mute-2* expressing MpICE2 at 9 DAS. Arrowheads
914 and asterisks indicate stomata and hydathode pores, respectively. **b**, Confocal images of
915 *A. thaliana* abaxial leaves of wild type (Col-0), *ice1-2 scrm2-1*, *proAtICE1:MpICE1 ice1-*
916 *2 scrm2-1*, and *proAtICE1:MpICE2 ice1-2 scrm2-1* at 13 DAS. Bars, 100 μ m.

917

918

919 **Supplementary Information**

920 Supplementary Tables 1 and 2

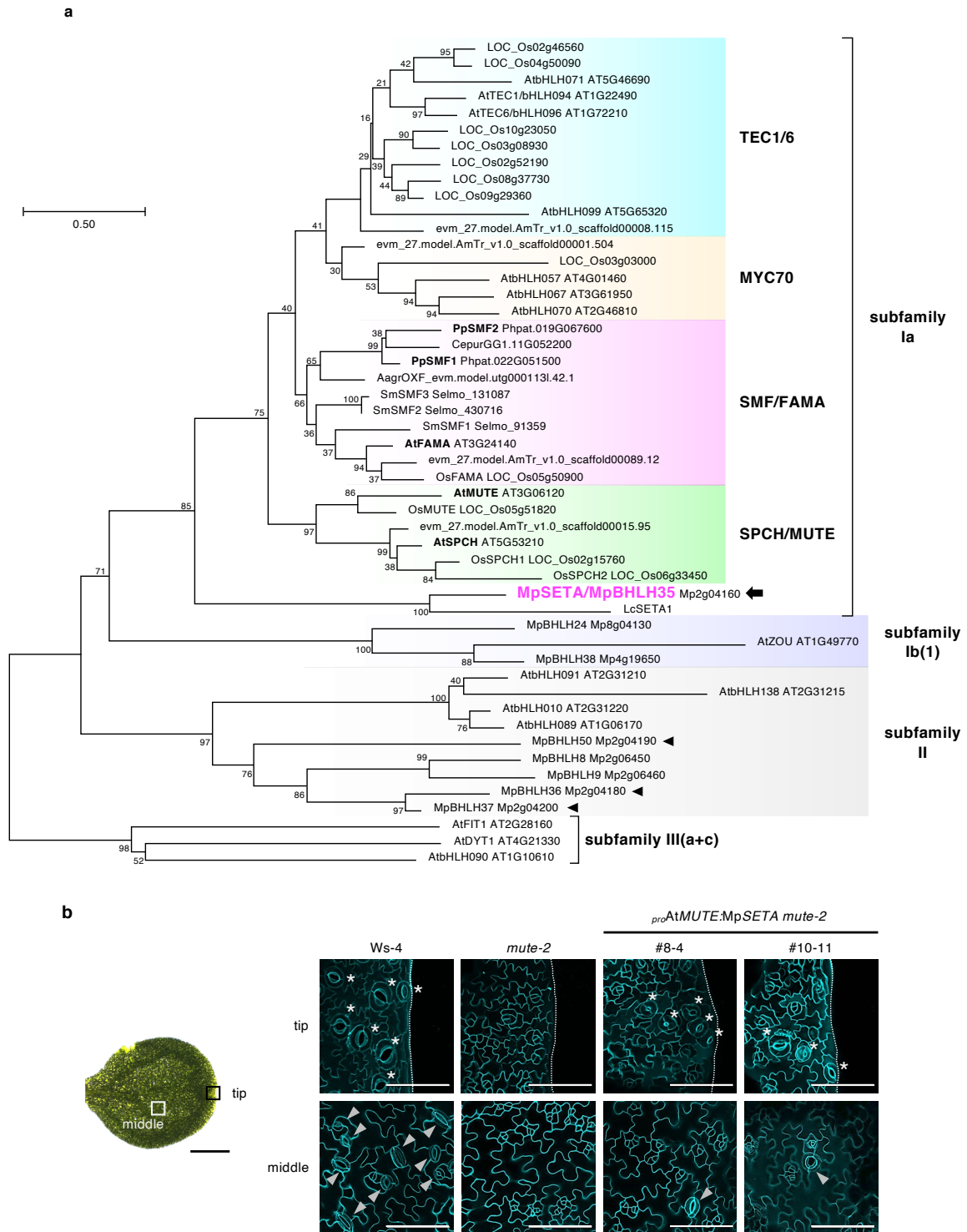


Fig. 1 | MpSETA is the only bHLH transcription factor that belongs to subfamily Ia in *M. polymorpha*. **a**, A maximum-likelihood bHLH phylogenetic tree of subfamilies Ia, Ib(1) (purple), II (gray), and III(a+c) (outgroup) is shown. Numbers at branches indicate bootstrap values calculated from 1,000 replicates. Ia bHLHs are divided into four groups: TEC1/6 clade (light blue), MYC70 clade (cream-yellow), SMF/FAMA clade (magenta), and SPCH/MUTE clade (green). Species are abbreviated as follows: Mp, *M. polymorpha* (liverwort); Lc, *L. cruciata* (liverwort); Pp, *P. patens* (moss); Cepur, *Ceratodon purpureus* (moss); Aagr, *Anthoceros agrestis* (hornwort); Sm, *Selaginella moellendorffii* (lycophyte); AmTr, *Amborella trichopoda* (basal angiosperm); Os, *Oryza sativa* (monocot); At, *A. thaliana* (dicot). An arrow indicates MpSETA/MpBHLH35 (Mp2g04160), and arrowheads indicate bHLH TFs mentioned as FAMA-like bHLH TFs in a previous study¹⁴. Amino acid sequences from only *A. thaliana* and *M. polymorpha* were used for subfamilies Ib(1), II, and III(a+c). **b**, Confocal images of *A. thaliana* abaxial cotyledons of wild type (Ws-4), *mute-2*, and *proAtMUTE:MpSETA mute-2* at 9 days after stratification (DAS). The upper panels and lower panels show the middle area and tip area of the cotyledons, respectively (left image). Arrowheads and asterisks indicate stomata and hydathode pores, respectively. Bars, 100 μ m (b, confocal images), and 1 mm (b, left).

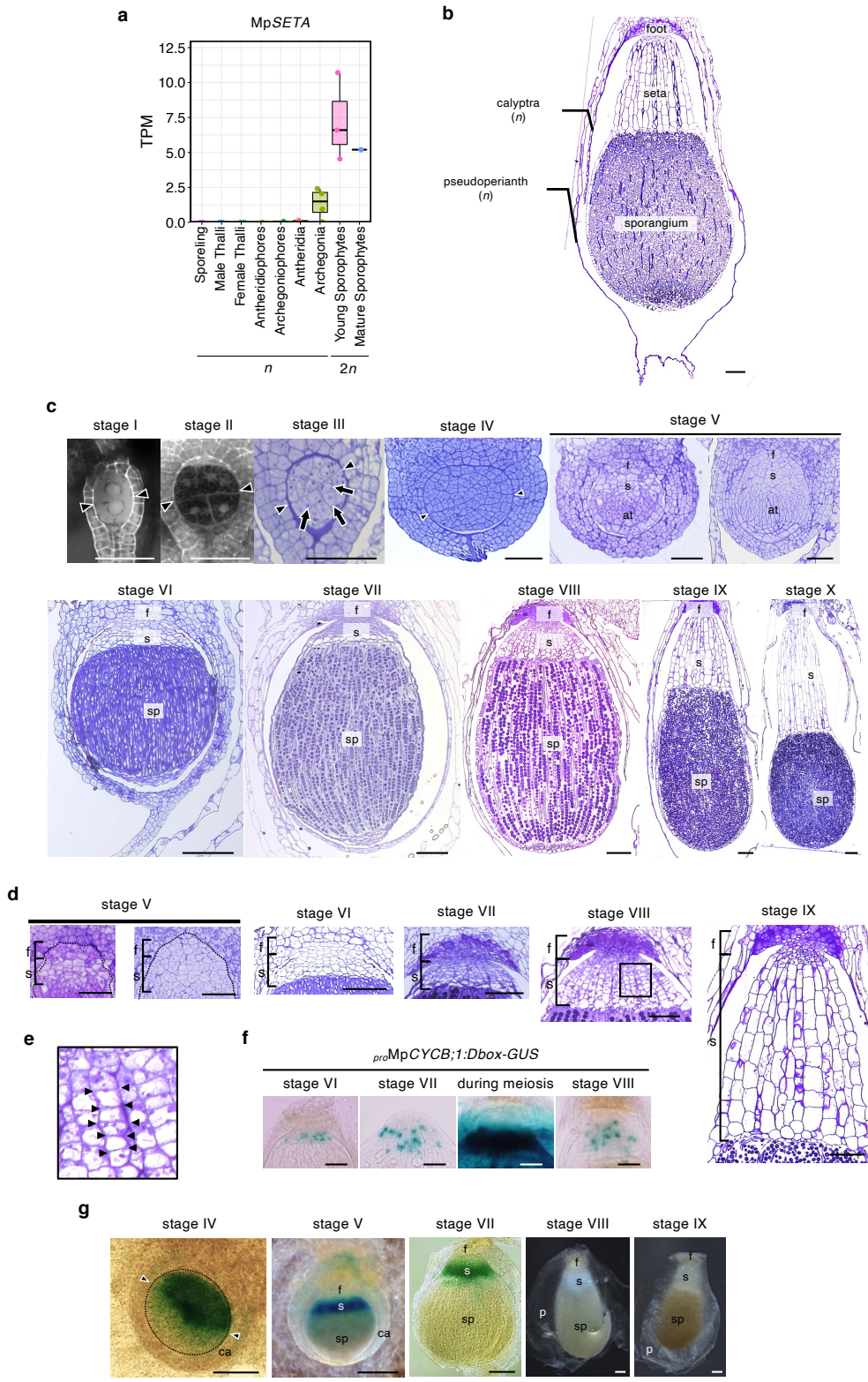


Fig. 2 | *MpSETA* is preferentially expressed in developing sporophyte. **a**, Box plot showing the expression profiles of *MpSETA* across nine *M. polymorpha* tissues. Y-axis shows transcripts per million (TPM). Sporeling and thalli are vegetative gametophytic (*n*) organs. Antheridiophores and archegoniophores are haploid male and female reproductive receptacles, respectively. Antheridia and archegonia are the organs that produce sperms and egg cells, respectively. Sporophytes are diploid (*2n*) organs developed after fertilization. **b**, Tissue section of mature *M. polymorpha* sporophyte (stage IX). **c**, Developmental stages of *M. polymorpha* sporophytes after 4–40 days' postfertilization. (I) sporophyte differentiating an epibasal cell and a hypobasal cell, (II) 4-cell or 8-cell sporophyte, (III) sporophyte differentiating amphithecium and endothecium, (IV) later globular sporophyte, (V) sporophyte differentiating foot, seta, and archesporial tissues, (VI) sporophyte differentiating sporogenous cells and elaterocytes (or elater mother cell), (VII) sporophyte differentiating sporocytes (or spore mother cells), (VIII) sporophyte differentiating spore tetrads after meiosis, (IX) mature sporophyte before the seta elongation, (X) mature sporophyte after seta elongation. Arrows indicate the endothecium. Arrowheads indicate the cell wall of the first cell division. **d**, Magnified images showing the foot and seta for each stage of wild-type sporophytes. Same images as used in (c). **e**, The formation of the cell files of seta in the wild type stage VIII sporophyte. Enlarged images of the square areas are shown in (d). Arrowheads indicate the plane of proliferative cell divisions. **f**, Histochemical detection of β -glucuronidase (GUS) activity in the sporophytes crossed with male wild type and female *proMpCYCB;1:Dbox-GUS*. **g**, Histochemical detection of β -glucuronidase (GUS) activity driven by *MpSETA* promoter in the developing seta region from stage IV to stage IX. f, foot; s, seta; at, archesporial tissue; sp, sporangium; ca, calyptra; p, pseudoperianth. Arrowheads indicate the cell wall of the first cell division. Bars, 50 μ m (c, top), 100 μ m (d and f), and 200 μ m (b, c, bottom, and g).

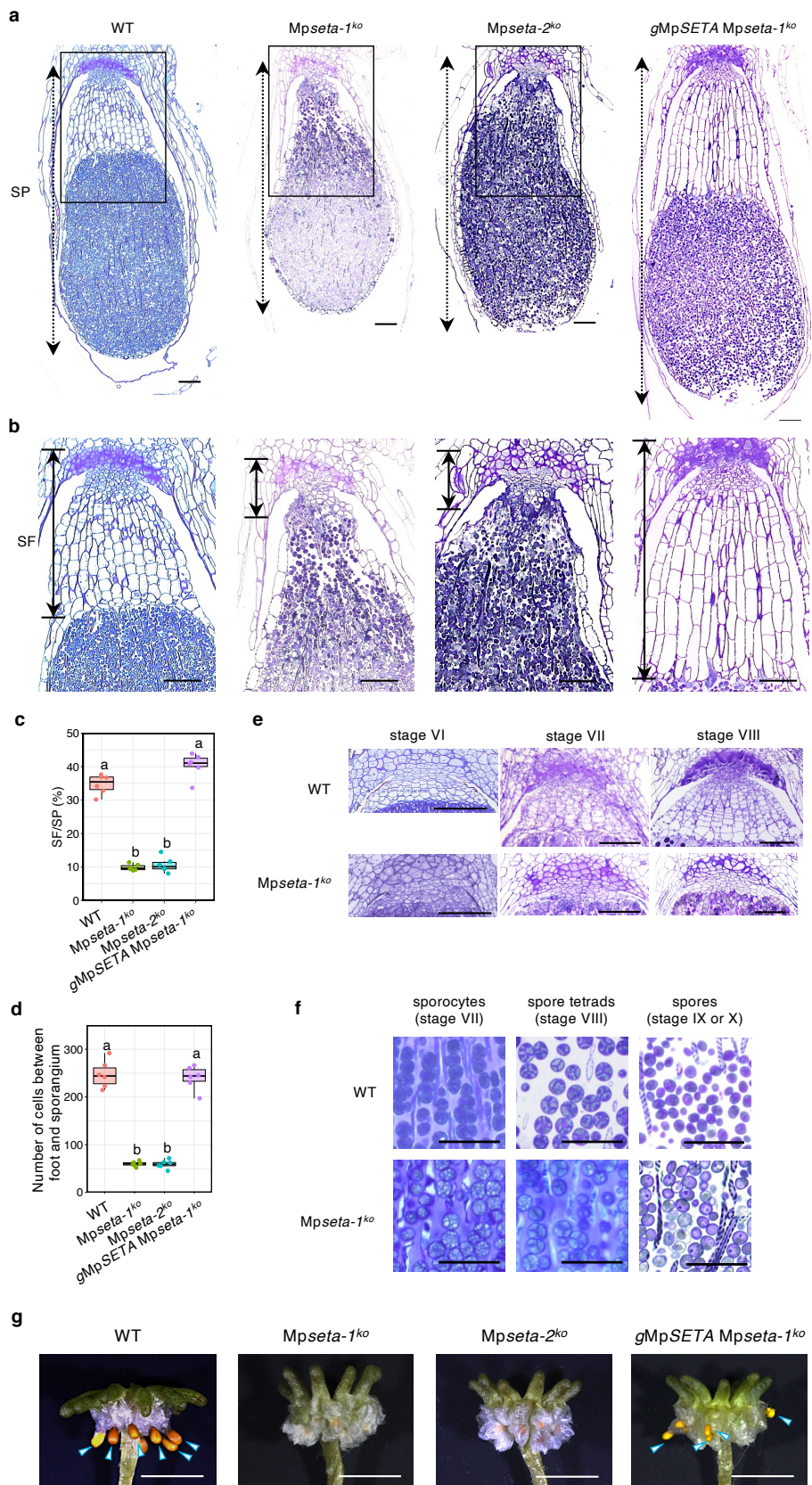


Fig. 3 | *Mpseta*^{ko} mutants show developmental defects in the seta. **a,b**, Longitudinal sections of sporophytes of indicated genotypes. Enlarged images of the square areas are shown in **(b)**. Dashed and solid arrows indicate the length of the sporophyte (SP) and the length from the boundary between gametophyte and sporophyte to the proximal side of sporangium (SF), respectively. **c,d**, Quantitative data showing the SF/SP length ratio and the number of cells in the seta region. Since the boundary between seta and foot is unclear, cells excluding transfer cells (the cells at the boundary between gametophyte and sporophyte) were used to count the number of cells. The different letters indicate significantly different mean values at $p < 0.01$ (Tukey's HSD test). ($n = 6$ independent lines). **e**, Comparative analyses of the tissue development between wild type and *Mpseta-1*^{ko}. Enlarged images of longitudinal sections of stage VI, stage VII and stage VIII sporophytes. **f**, Sporogenesis process in wild type and *Mpseta-1*^{ko}. Sporocytes are the cells before the pre-meiotic stage, and spore tetrads are the cells immediately after meiosis. **g**, One month-post-fertilization archegoniophores that produce mature sporophytes. Arrowheads indicate sporangia exposed to the outside of calyptra due to elongation of seta cells. Bars, 50 μm (**f**), 100 μm (**e**), 200 μm (**a** and **b**), and 5 mm (**e**).

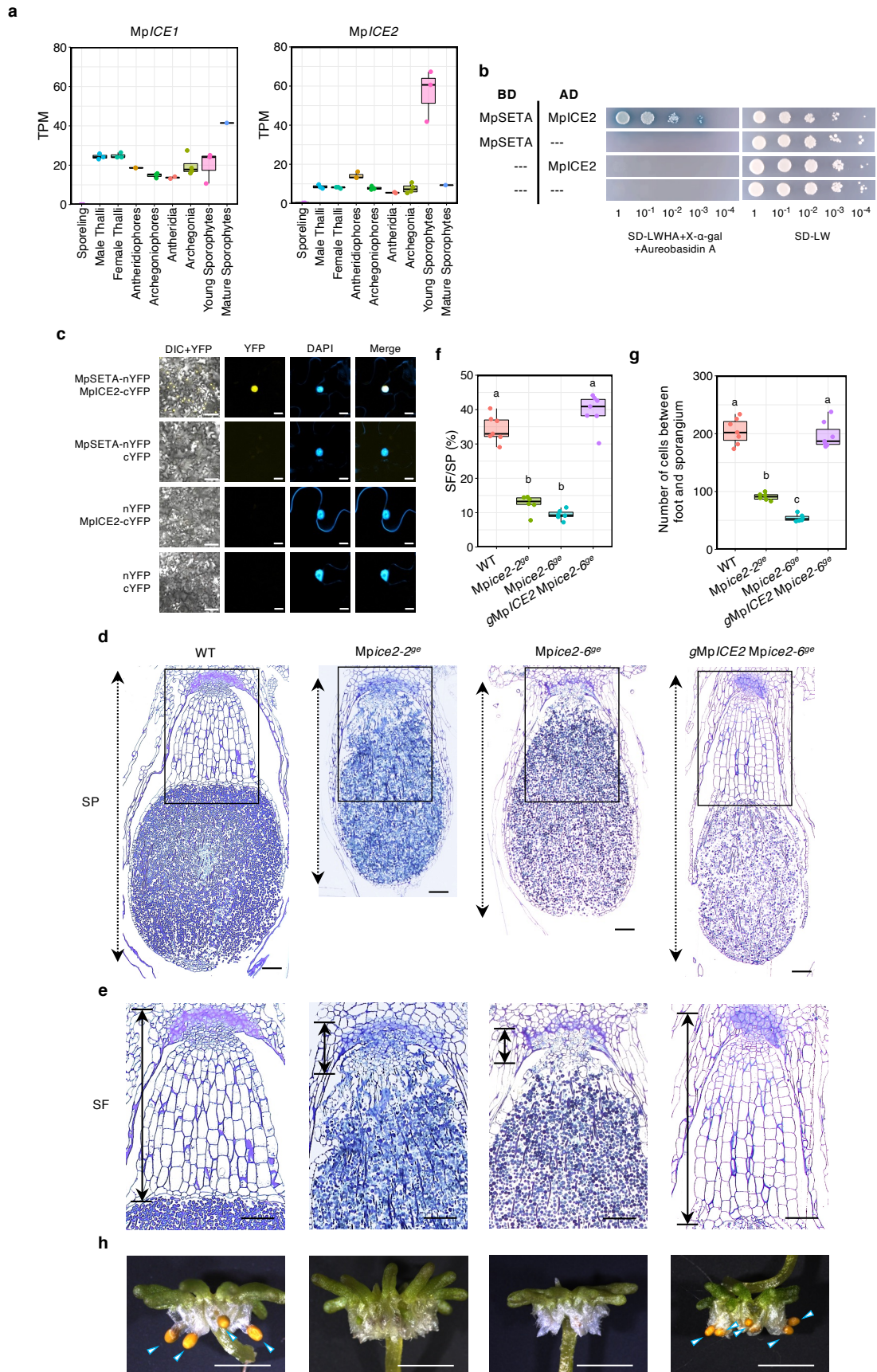


Fig. 4 | MpICE2 regulates setal development in cooperation with MpSETA. **a.** Box plot showing the expression profiles of MpICE1 and MpICE2 across nine *M. polymorpha* tissues. Y-axis shows transcripts per million (TPM). **b.** Y2H assays showing the interaction between MpSETA and MpICE2. MpSETA fused with GAL4 DNA-binding domain (DBD) was used as bait, while MpICE2 fused with GAL4 activation domain (AD) was used as prey. DBD alone and AD alone were used as the negative control. **c.** BiFC assays showing the interaction between MpSETA and MpICE2 in *N. benthamiana* leaf epidermal cells. MpSETA was fused to the N-terminal fragment of EYFP (nYFP), while MpICE2 was fused to the C-terminal fragment of EYFP (cYFP). nYFP alone and cYFP alone were used as the negative control. Nuclei were stained by 4',6-diamidino-2-phenylindole (DAPI). **d,e.** Longitudinal sections of sporophytes of indicated genotypes. Enlarged images of the square areas are shown in **(e)**. Dashed and solid arrows indicate the length of the sporophyte (SP) and the length from the boundary between gametophyte and sporophyte to the proximal side of sporangium (SF), respectively. **f,g.** Quantitative data showing the SF/SP length ratio and the number of cells in the seta region. Since the boundary between seta and foot is unclear, cells excluding transfer cells (the cells at the boundary between gametophyte and sporophyte) were used to count the number of cells. The different letters indicate significantly different mean values at $p < 0.01$ (Tukey's HSD test) ($n = 6$ or 7 independent lines). **h.** One month-post-fertilization archegoniophores that produce mature sporophytes. Arrowheads indicate sporangia exposed to the outside of calyptra due to elongation of seta cells. Bars, 10 μm (**c**, YFP, DAPI, and Merge), 100 μm (**c**, left, **d**, and **e**), and 5 mm (**f**).

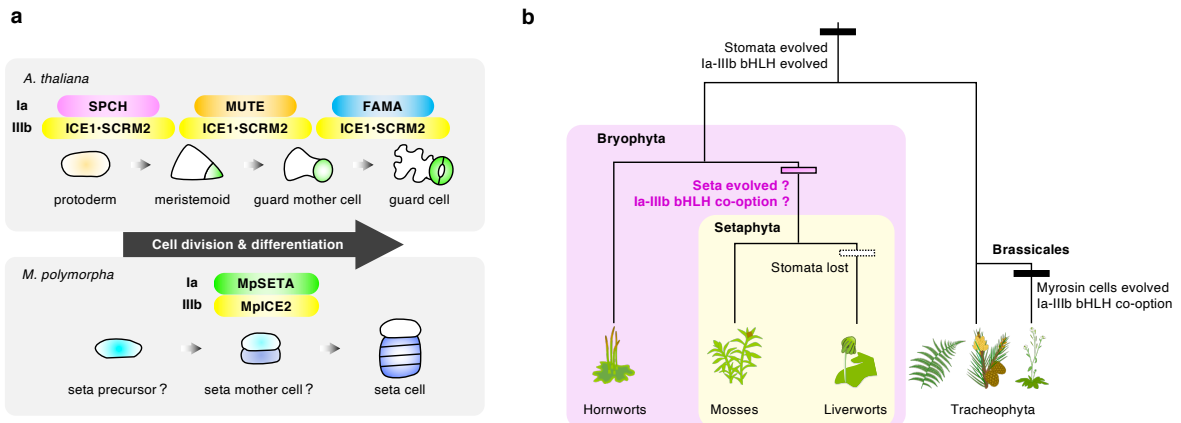
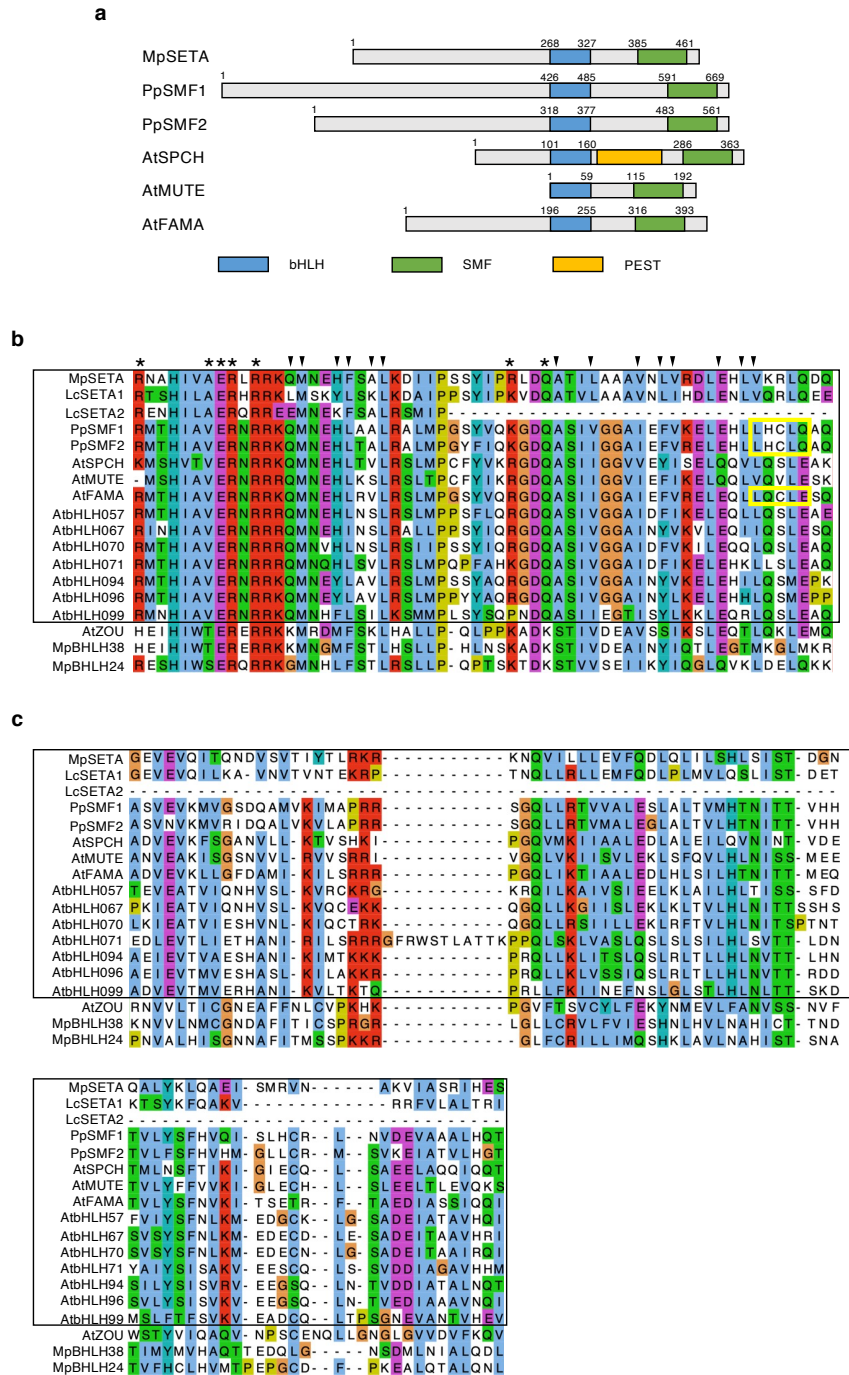
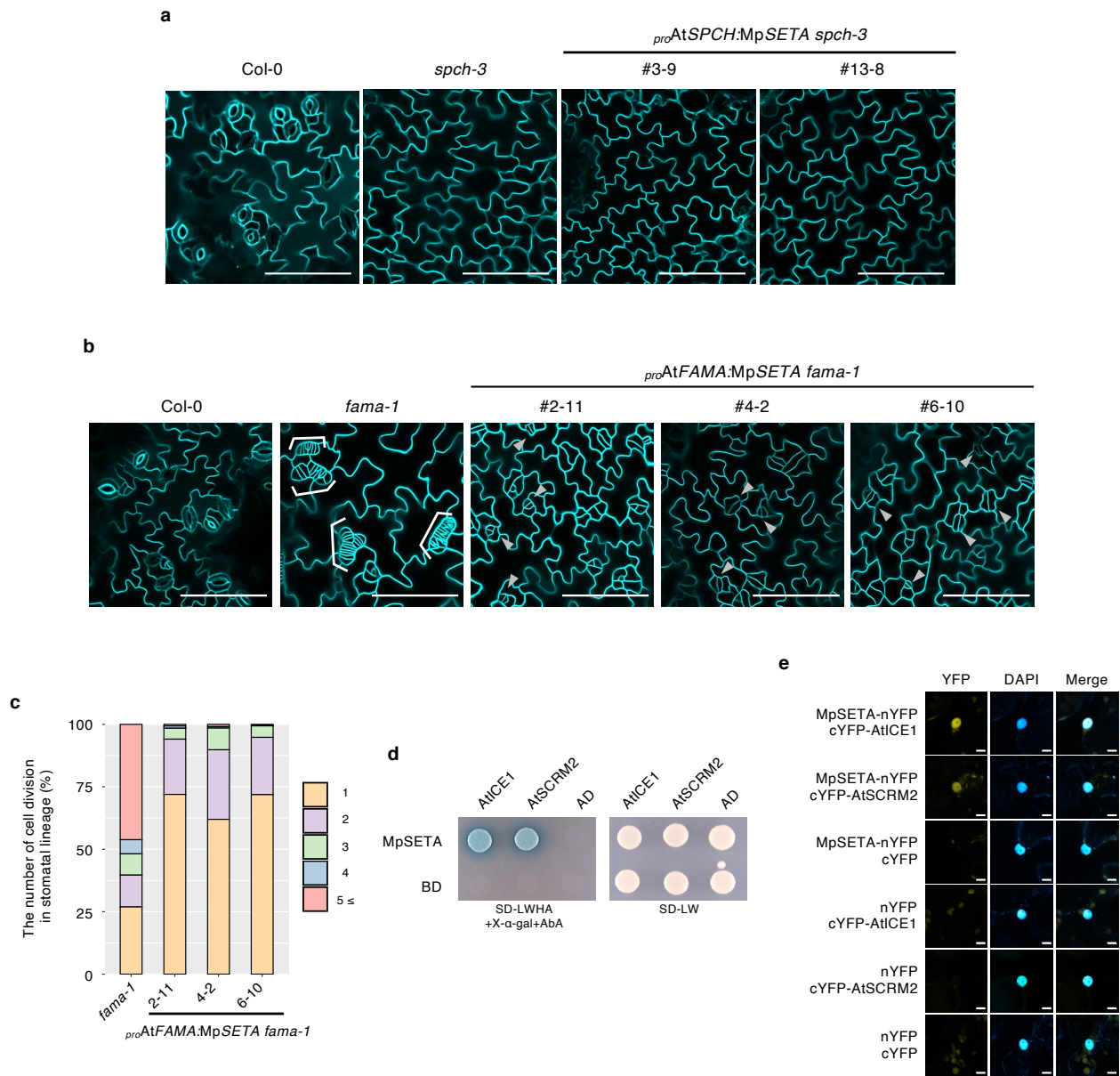


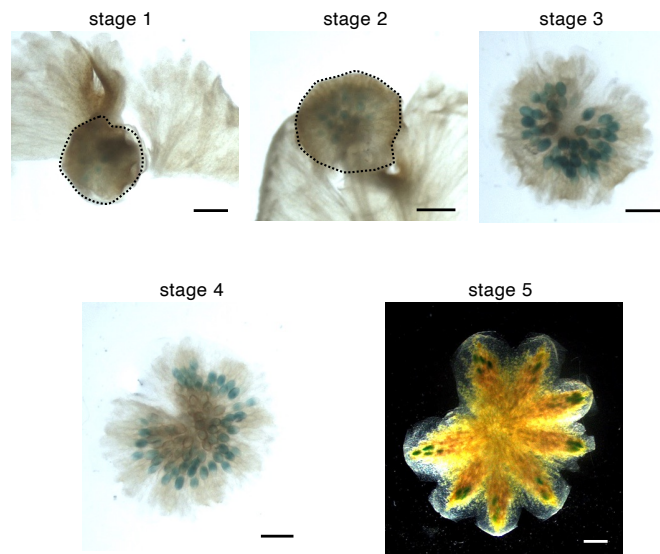
Fig. 5 | Function and co-option of the la-IIIb bHLH module during the evolution of land plants. a, Schematic model comparing the molecular functions of the la-IIIb bHLH TF modules in *A. thaliana* and *M. polymorpha* during cell fate determination. In *A. thaliana*, the heterodimer of la bHLHs (SPCH, MUTE, and FAMA) and IIIb bHLHs (ICE1 and SCRM2) control the development of stomata. In *M. polymorpha*, the heterodimer of la bHLH (MpSETA) and IIIb bHLH (MpICE2) regulates cell differentiation and cell division in the seta precursor transition and might directly or indirectly be involved in the symmetric division of a putative seta mother cell. **b**, An evolutionary model for the la-IIIb bHLH TF module. Co-option of the la-IIIb bHLH module might have occurred multiple times independently during the evolution of land plants. First, stomata and a transcriptional module consisting of la-IIIb bHLHs evolved in the common ancestor of land plants. In the ancestral plant, the la bHLHs may have had MUTE- and FAMA-like functions. Second, the la-IIIb bHLH TF module might have been co-opted to regulate setal development in the ancestor of the Setophyta. Third, after mosses and liverworts diverged, the common ancestor of liverworts lost its stomata. A co-option of the la-IIIb bHLH module occurred in the Brassicales plants for regulating myrosin idioblast development.



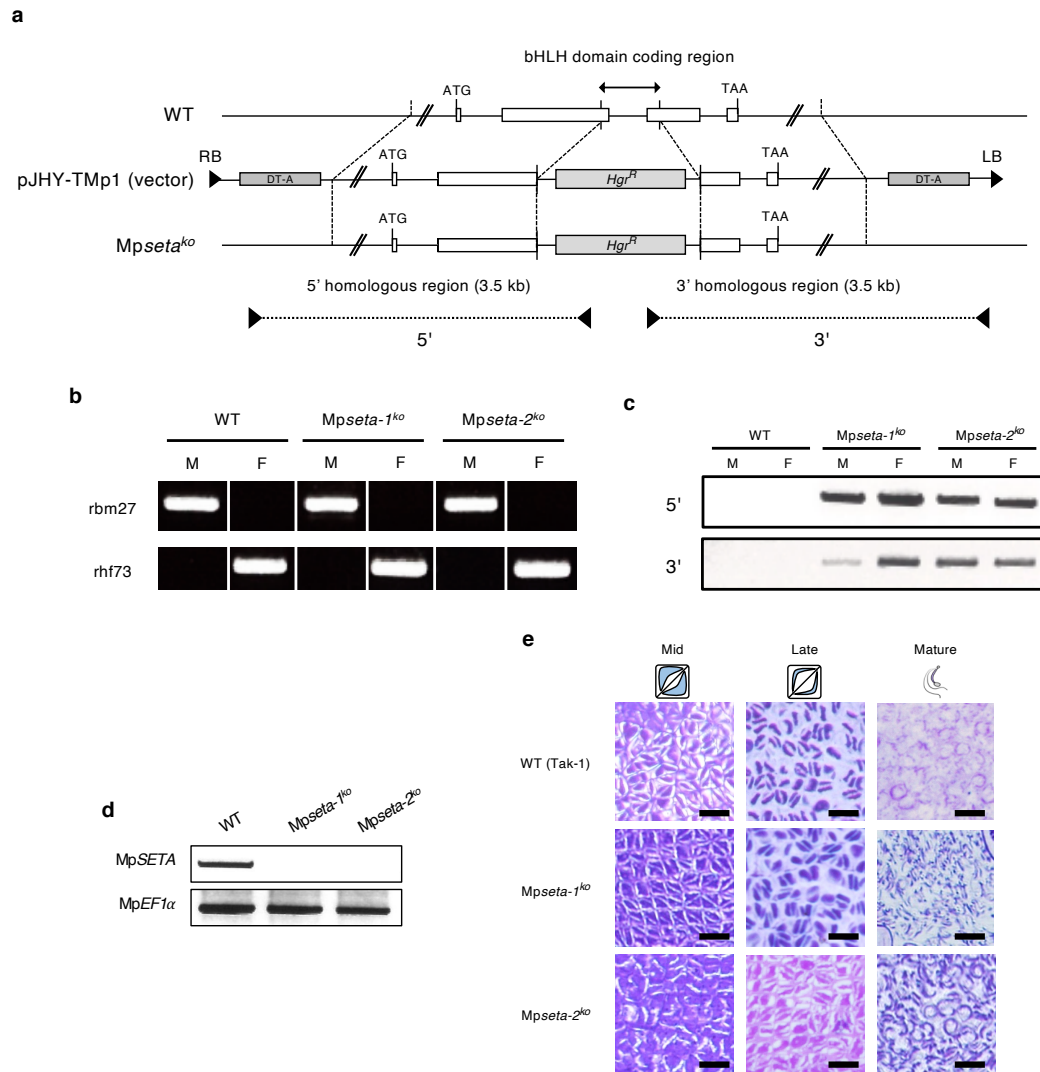
Extended Data Fig. 1 | Comparison of the domain architecture of la bHLHs in land plants. a, A diagram of the domain architecture of MpSETA (*M. polymorpha*), PpSMF1, PpSMF2 (*P. patens*), AtSPCH, AtMUTE, and AtFAMA (*A. thaliana*). While no PEST domain was identified, MpSETA has a bHLH domain and SMF domain conserved at the C-terminus like other la bHLH proteins. SMF domain is structurally considered to be the ACT-like domain, which is a putative domain for protein-protein dimerization. **b**, Sequence alignment of the bHLH domain of la bHLH proteins. la bHLHs are surrounded by a black box, and others are lb(1) bHLHs. Asterisks indicate amino acids that are assumed to be important for binding to the E-box (CANNTG), and the triangles indicate amino acids that are assumed to be important for dimerization of the bHLH domain. The yellow box indicates the LxCxG motif, which is a binding motif with Retinoblastoma-related (RBR). **c**, Sequence alignment of the C-terminal SMF domain of la bHLH proteins.



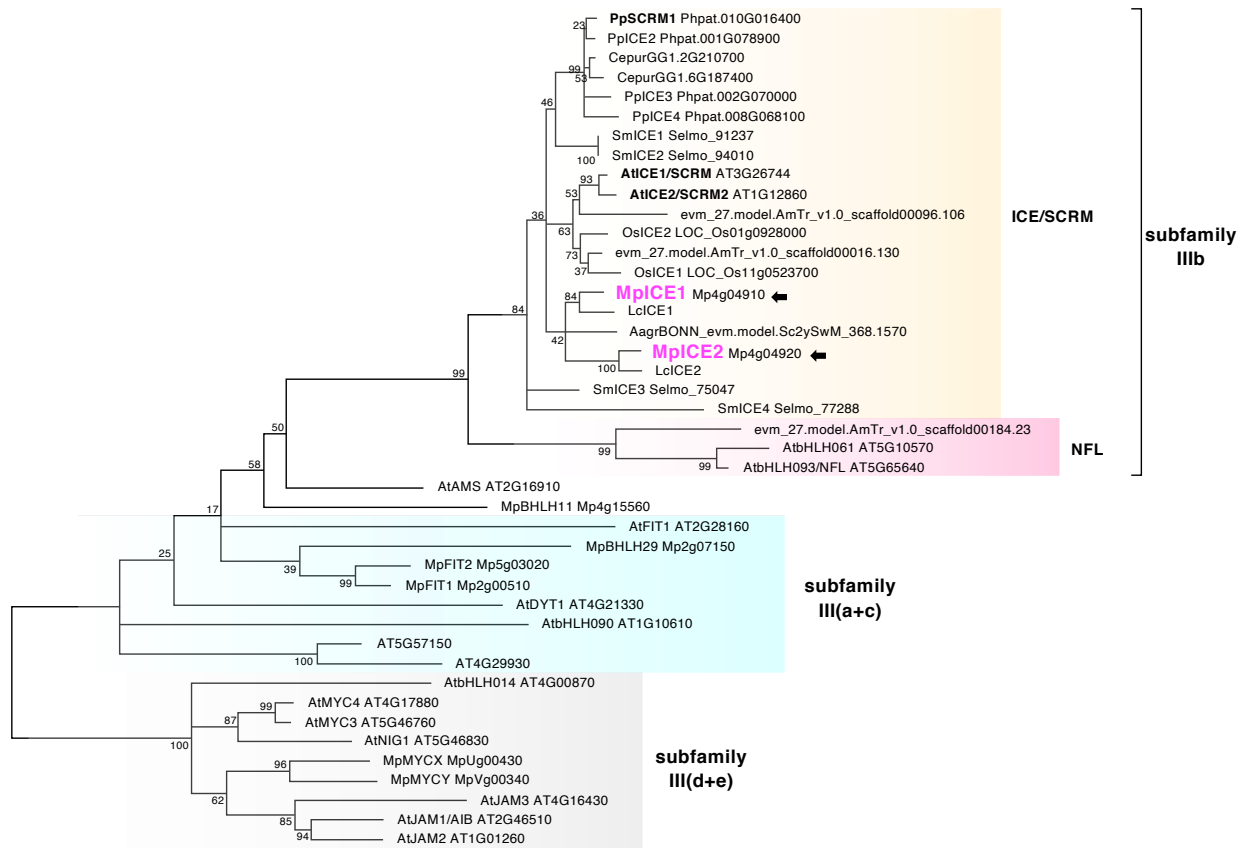
Extended Data Fig. 2 | Function of MpSETA in *A. thaliana* la bHLH mutants. **a**, Confocal images of *A. thaliana* abaxial cotyledons of wild type (Col-0), *spch-3*, and *proAtSPCH:MpSETA spch-3* at 9 days after stratification (DAS). **b**, Confocal images of *A. thaliana* abaxial cotyledons of wild type (Col-0), *fama-1*, and *proAtFAMA:MpSETA fama-1* at 9 DAS. Brackets and arrows indicate *fama* tumors and stomatal-lineage cells, respectively. **c**, Quantitative data of the distribution of the number of cell divisions that occurred in the stomatal lineage in each genotype. ($n > 320$ cells per genotype, 9 DAS cotyledons). **d**, Y2H assays in which the MpSETA fused with GAL4 DNA-binding domain (DBD) was used as bait, and the AtICE1 and AtSCRM2 fused with GAL4 activation domain (AD) were used as prey. DBD alone and AD alone were used as the negative controls. **e**, BiFC assays showing the interaction between MpSETA and AtICE1 or AtSCRM2 in *N. benthamiana* leaf epidermal cells. MpSETA was fused to the N-terminal fragment of EYFP (nYFP), while AtICE1 or AtSCRM2 was fused to the C-terminal fragment of EYFP (cYFP). nYFP alone and cYFP alone were used as the negative control. Nuclei were stained by DAPI. Bars, 10 μ m (**e**), and 100 μ m (**a,b**).



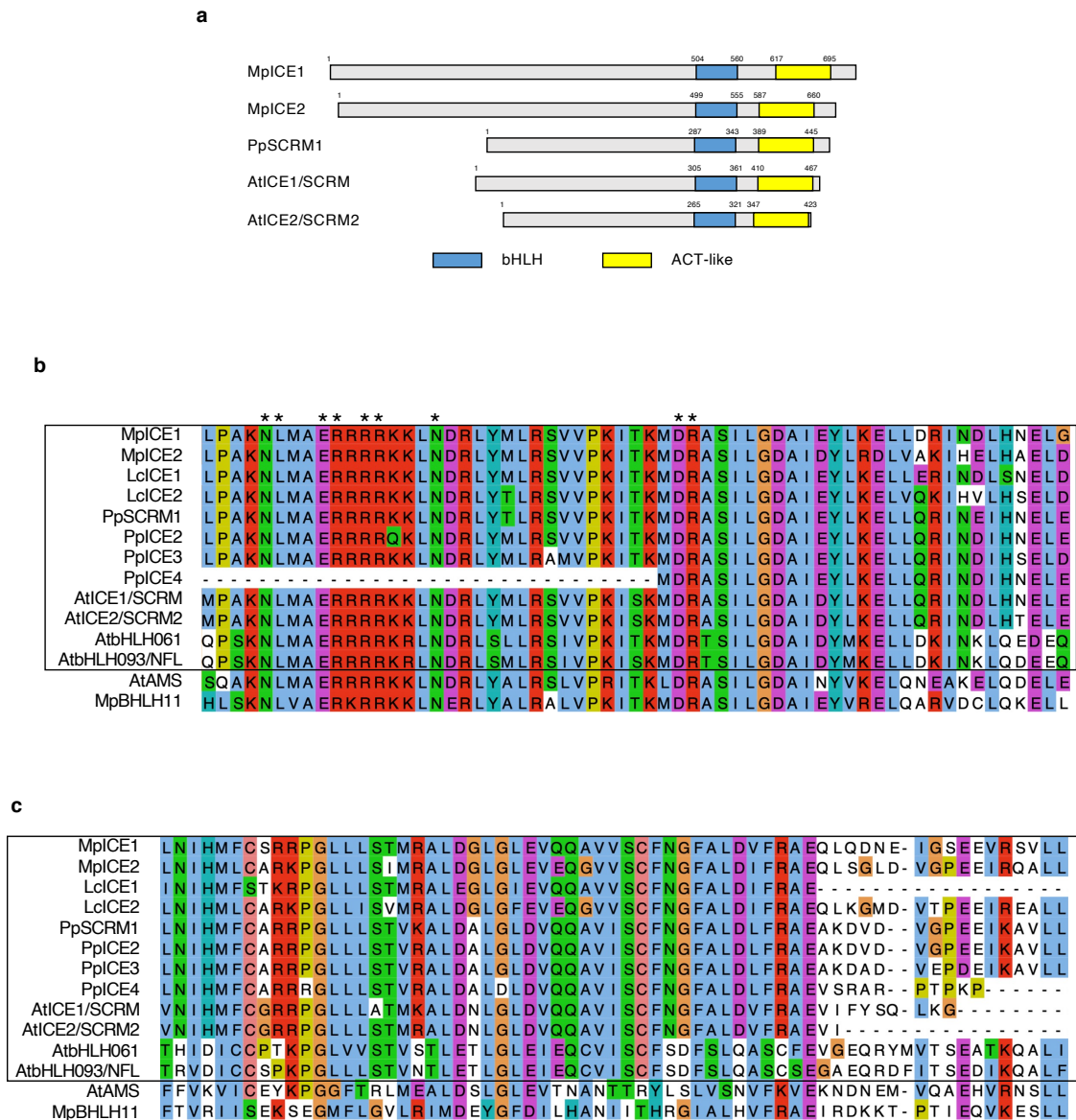
Extended Data Fig. 3 | Expression analysis of *MpSETA* in the gametophytic tissues. Histochemical detection of β -glucuronidase (GUS) activity driven by *MpSETA* promoter in the developing antheridia. Bars, 1 mm.



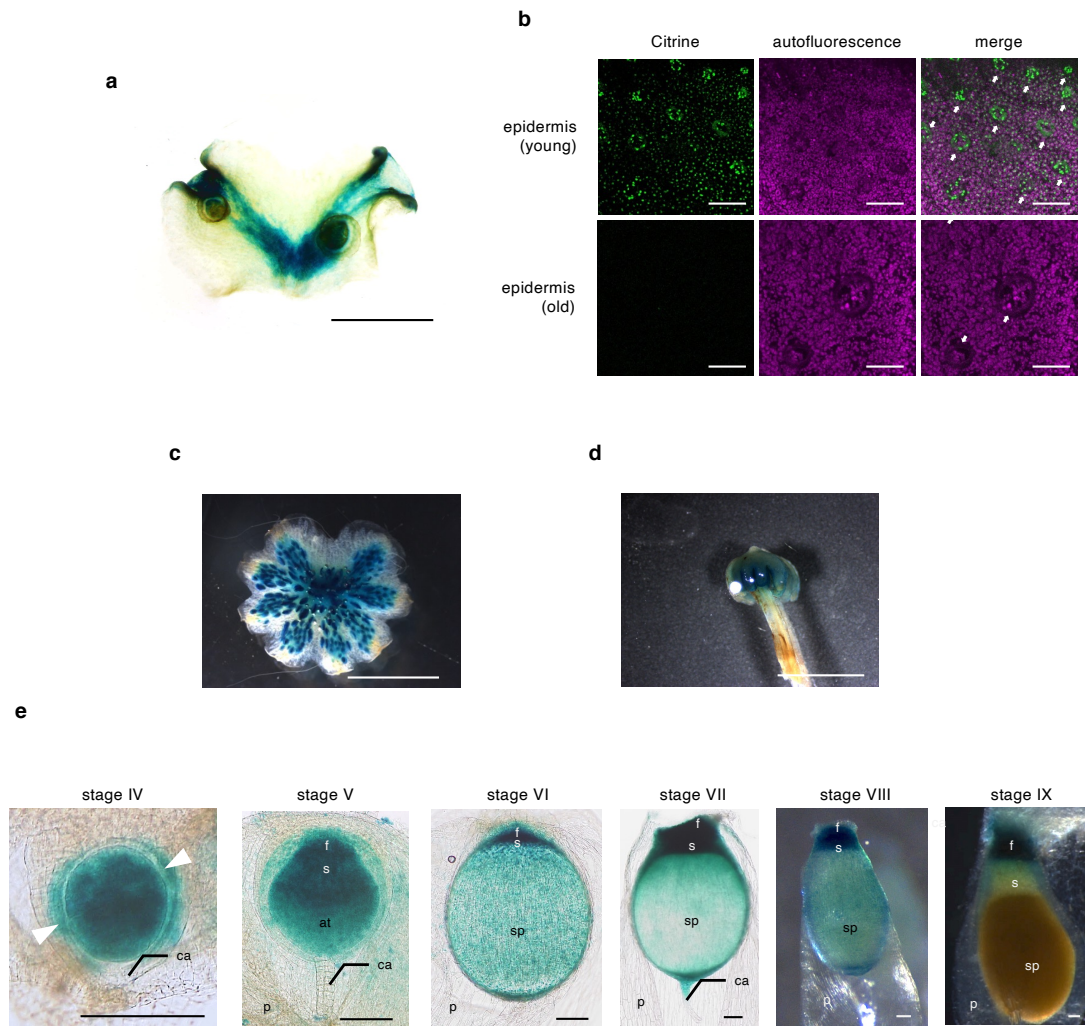
Extended Data Fig. 4 | Generation and phenotypes of MpSETA knock-out lines. a, Structure of the MpSETA locus disrupted by homologous recombination. Knock-out lines have a deletion in the bHLH domain coding region. White boxes indicate the exons of the MpSETA coding sequence. DT-A, diphtheria toxin A fragment gene; *Hgr^R*, hygromycin resistant gene. **b**, Genotyping of the *Mpseta^{ko}* lines used in this study to distinguish the sex. *rbm27*, a male-specific marker; *rhf73*, a female-specific marker. **c**, Genotyping of the *Mpseta^{ko}* lines. The position of primers used for PCR is shown in (a). M, Male; F, Female. **d**, RT-PCR to confirm the loss of the full-length MpSETA transcript in *Mpseta^{ko}* lines in 21 DPF sporophytes. *MpEF1 α* was used as an internal control. **e**, Spermatogenesis process in WT and *Mpseta^{ko}* lines. All images are at the same scale. Bars, 10 μ m (e).



Extended Data Fig. 5 | Phylogenetic tree of IIIb bHLH TFs. A maximum-likelihood bHLH phylogenetic tree of subfamilies IIIb, III (a+c) (light blue), and III(d+e) (outgroup) is shown. Numbers at branches indicate bootstrap values calculated from 1,000 replicates. IIIb bHLHs are divided into 2 groups: ICE/SCRM clade (orange) and NFL clade (magenta). Species are abbreviated as follows: Mp, *M. polymorpha* (liverwort); Lc, *L. cruciata* (liverwort); Pp, *P. patens* (moss); Cepur, *Ceratodon purpureus* (moss); Agr, *Anthoceros agrestis* (hornwort); Sm, *Selaginella moellendorffii* (lycophyte); AmTr, *Amborella trichopoda* (basal angiosperm); Os, *Oryza sativa* (monocot); At, *A. thaliana* (dicot). Arrows indicate MpICE1 (Mp4g04910) and MpICE2 (Mp4g04920). For the phylogenetic construction of subfamilies III(a+c) and III(d+e), we used the amino acid sequences from only *A. thaliana* and *M. polymorpha*.



Extended Data Fig. 6 | Comparison of the domain architecture of IIIb bHLHs in land plants. a, A diagram of the domain architecture of MpICE1, MpICE2 (*M. polymorpha*), PpSCRM1 (*P. patens*), AtICE1, and AtSCRM2 (*A. thaliana*). MpICE1 and MpICE2 have a bHLH domain and ACT-like domain conserved at the C-terminus like other IIIb bHLH proteins. **b**, Sequence alignment of the bHLH domain of IIIb bHLH proteins. IIIb bHLHs are surrounded by a black box, and others are outgroup. Asterisks indicate amino acids that are assumed to be important for binding to the E-box (CANNTG). **c**, Sequence alignment of the C-terminal ACT-like domain of IIIb bHLH proteins.



Extended Data Fig. 7 | The expression analysis of *MpICE2*. **a**, Histochemical detection of β -glucuronidase (GUS) activity driven by *MpICE2* promoter in the vegetative thallus. **b**, Confocal images of the dorsal epidermis of *proMpICE2:Citrine-GUS-NLS* line. Upper and lower panels indicate the epidermis around the apical notch and the epidermis around the midrib, respectively. Arrows indicate the air pores. **c,d**, Histochemical detection of GUS activity driven by *MpICE2* promoter in the gametophytic reproductive organs. An antheridiophore (**c**) and an archegoniophore (**d**) are shown. **e**, Expression pattern of *MpICE2* in the developing sporophytes. f, foot; s, seta; at, archesporial tissue; sp, sporangium; ca, calyptra; p, pseudoperianth (*n*). Arrowheads indicate the cell wall of the first cell division. Bars, 5 mm (**c** and **d**), 100 μ m (**b** and **e**).

a

MpICE2 (Mp4g04920)



```

GCAAAAAAGGCTTGCCTGCGAAGAATC...TGGCAGAA
GCAAAAAAGGCTTGCCTGCGAAGAATC...TGGCAGAA
WT (Tak-1) GCAAAAAAGGCTTGCCTGCGAAGAATCTCATGGCAGAA
WT (Tak-2) GCAAAAAAGGCTTGCCTGCGAAGAATCTCATGGCAGAA
Mpice2-29e (Male) GCAAAAAAGGCTTGCCTGCGAAGAATCATTGGCAGAA
Mpice2-29e (Female) GCAAAAAAGGCTTGCCTGCGAAGAATCATTGGCAGAA

ACAGAGCATCAATcctTGGGATCCCCATCAATCTGGGACGCAATCGA
ACAGAGCATCAATNNNTGGGANNNNNNNNNNNNNNNNNNNNNNCGCAATCGA
WT (Tak-1) ACAGAGCATCAATCCTTGGGGA-----CGCAATCGA
WT (Tak-2) ACAGAGCATCAATCCTTGGGGA-----CGCAATCGA
Mpice2-69e (Male) ACAGAGCATCAAT---TGGGATCCCCATCAATCTGGGACGCAATCGA
Mpice2-69e (Female) ACAGAGCATCAAT---TGGGATCCCCATCAATCTGGGACGCAATCGA
                                3 bp                17 bp

```

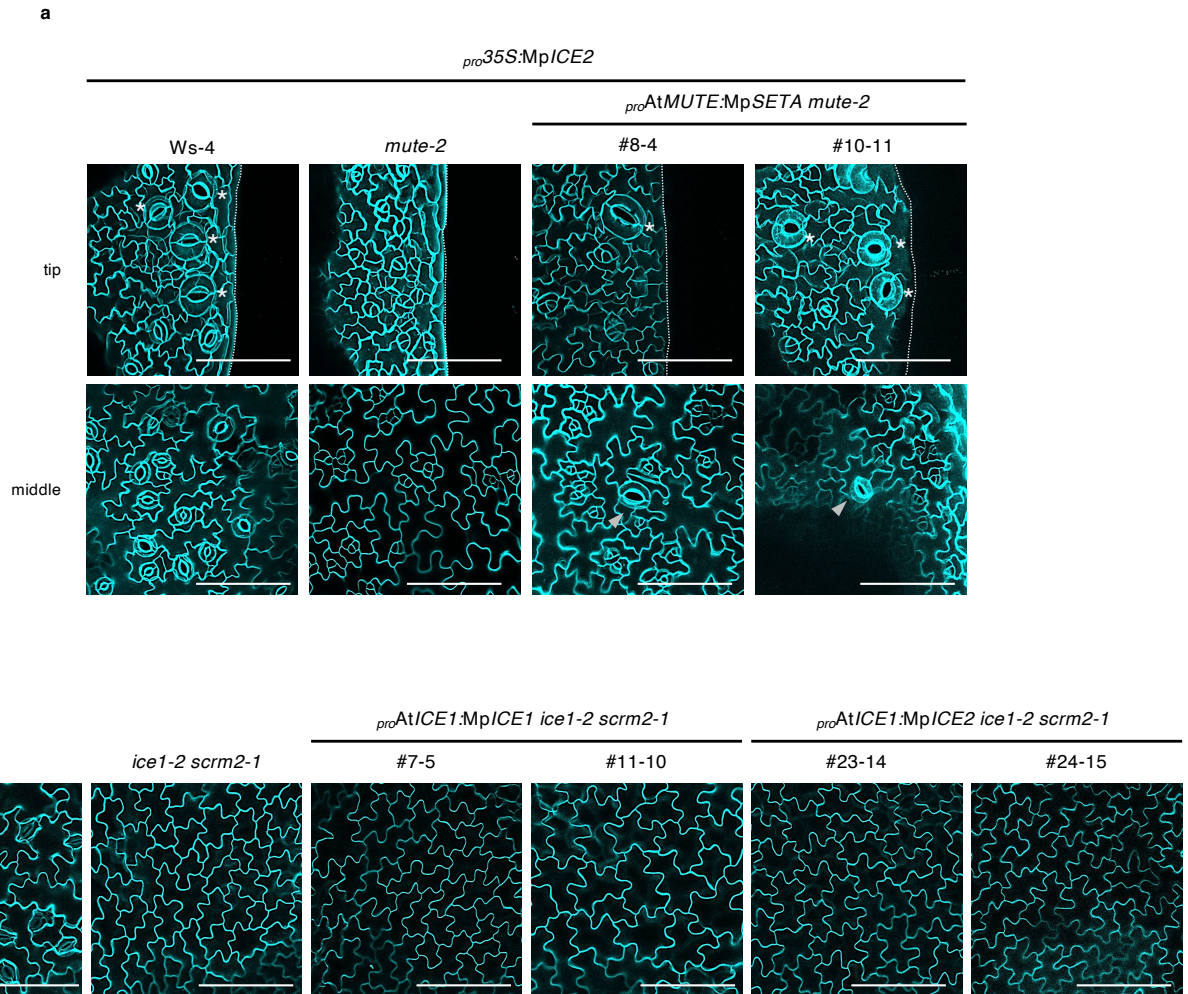
b

```

      * *      * *      *
WT    P A K N L M A E R R R R K K L N D R L Y M L R S V V P K I T K M D R A S I L G D A I D Y L R D L V A K I H E L H A E L D
Mpice2-29e P A K N H L A E R R R R K K L N D R L Y M L R S V V P K I T K M D R A S I L G D A I D Y L R D L V A K I H E L H A E L D
Mpice2-69e P A K N L M A E R R R R K K L N D R L Y M L R S V V P K I T K M D R A S I G - - - - -

```

Extended Data Fig. 8 | Generation of Mpice2 mutants by CRISPR/Cas9. a, Schematic representation of the MpICE2 gene and the resulting mutations in the obtained CRISPR/Cas9-generated alleles. Gray, white, and blue boxes indicate the coding sequences (CDS), the untranslated regions (UTR), and the bHLH domain coding region, respectively. **b,** Sequence alignment of putative translational products of wild type and Mpice2^{29e} mutants. Asterisks indicate the amino acids that are assumed to be important for binding to E-box.



Extended Data Fig. 9 | Functional analysis of MpICE1 and MpICE2 in *A. thaliana* mutants. a, Confocal images of *A. thaliana* abaxial cotyledons of wild type (*Ws-4*), *ice1-2 scrm2-1*, and *proAtMUTE:MpSETA mute-2* expressing MpICE2 at 9 DAS. Arrowheads and asterisks indicate stomata and hydathode pores, respectively. **b**, Confocal images of *A. thaliana* abaxial leaves of wild type (Col-0), *ice1-2 scrm2-1*, *proAtICE1:MpICE1 ice1-2 scrm2-1*, and *proAtICE1:MpICE2 ice1-2 scrm2-1* at 13 DAS. Bars, 100 μ m.